

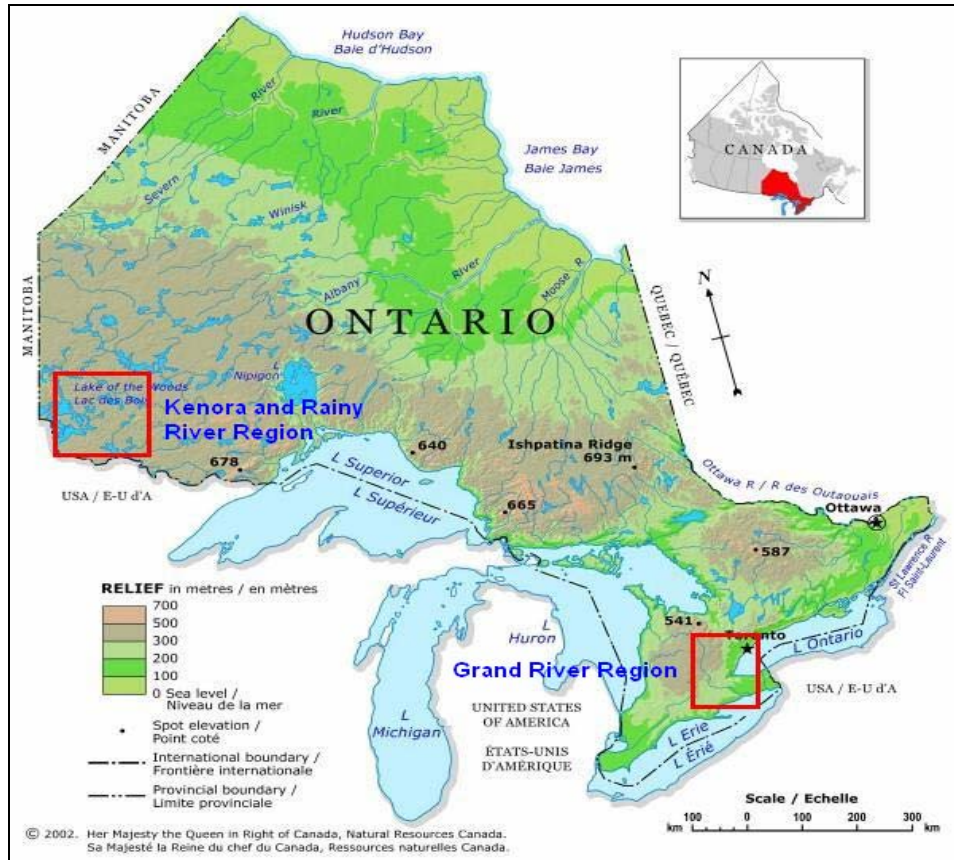
# Identification of the Effect of Climate Change on Future Design Standards of Drainage Infrastructure in Ontario

June 2005

Prepared by  
Paulin Coulibaly and Xiaogang Shi

McMaster University  
Department of Civil Engineering  
1280 Main Street West  
Hamilton, Ontario, Canada L8S 4L7  
Tel: (905) 525-9140; Fax (905) 529-9688

# Identification of the Effect of Climate Change on Future Design Standards of Drainage Infrastructure in Ontario



## Final Report

by

Paulin Coulibaly and Xiaogang Shi

Financial Support:  
Ministry of Transportation of Ontario  
Highway Infrastructure Innovation Funding Program

June 2005

---

# Table of Contents

---

<b>Executive Summary</b> .....	<b>iii</b>
<b>Introduction</b> .....	<b>1</b>
A. Statement of the Problem .....	1
B. Background .....	1
C. Research Objectives .....	3
D. Organization of the Report.....	4
<b>Study Areas and Data Used</b> .....	<b>5</b>
A. Study Areas .....	5
B. Data Collection .....	8
<b>Precipitation Trend Analysis</b> .....	<b>10</b>
A. Mann-Kendall Trend Test .....	10
B. Precipitation Trend analysis.....	12
C. Identifying Trends in Observed Precipitation Using IDF Curves .....	13
D. Summary of Trend Analysis Results.....	21
<b>Downscaling Daily Precipitation</b> .....	<b>22</b>
A. Statistical Downscaling Model .....	22
B. Downscaling Model Validation Results .....	25
C. Downscaling CGCM2 Outputs for the Future Period .....	29
<b>Comparison of IDF Curves</b> .....	<b>32</b>
A. Comparison of IDF Curves for the Current Period .....	32
Grand River Region .....	32
Kenora and Rainy River Region.....	36
B. Comparison of IDF Curves for the Future Period .....	39
Grand River Region .....	39
Kenora and Rainy River Region.....	44
C. Summary of the IDF Curves Comparison .....	49
<b>Rational Method Design of Highway Drainage Infrastructure</b> .....	<b>50</b>
A. Design Procedure .....	50
B. Case Study.....	51
Grand River Region .....	51
Kenora and Rainy River Region.....	53
<b>Summary and Conclusions</b> .....	<b>55</b>
<b>Recommendations</b> .....	<b>57</b>
<b>Acknowledgements</b> .....	<b>58</b>

References..... 59  
Appendix ..... 61

# Executive Summary

---

The intent of this research project is to identify the effect of climate change on future highway drainage infrastructures in Ontario. The reason is that drainage infrastructures have always been designed on the premise that the current climate is not changing and that historical climate data can be effectively used to predict future drainage design requirements. However, recent climate change impact studies indicate an increase in the intensity and frequency of extreme rainfall events. This raises an important question whether new drainage design standards should be established in order to include anticipated climate change effects.

First of all, the emphasis in this report was given to identify the trends of the observed precipitation data. By using the Mann-Kendall trend test, increasing trends in the annual maximum daily precipitation data of the Grand River Region and the Kenora and Rainy River Region are shown. In general, there are increased trends for three of the four stations selected in the Grand River Region and for all the four stations in the Kenora and Rainy River Region.

Given the coarse resolution of Canadian Global Circulation Models (CGCM), downscaling is necessary to obtain appropriate local scale information (precipitation series) representing the future climate conditions in the selected study areas. A statistical downscaling model (SDSM) is successfully used to downscale CGCM2 outputs for the current and future time periods. This permits to estimate the local and regional values of future daily precipitation and its variability very well.

Furthermore, the intensity-duration-frequency (IDF) curves analysis and comparison based on the downscaled data at each station shows significant changes in the precipitation intensity between the current and the future time periods. At almost all the stations, similar increasing trends are shown from the current to the 2080s time period except for the 2020s where there is a decrease. It is shown that most of the highway infrastructures can be significantly affected by the heavy and more frequent rainfall intensity predicted in the study areas. An actual 10-year drainage system will be able to withstand only 5-year storms by 2050s, whereas a current 50-year drainage structure will be able to handle only 20-year storms by 2050s. To further assess the potential impact of the predicted climate conditions, two design experiments are considered based on current and predicted precipitation data in the two study areas. The experiment results indicate significant changes in the design discharge and the corresponding pipe diameter necessary to safely drain the peak flow. It is suggested that an increase of about 16% in pipe diameter would be necessary for all sewer pipes in order to maintain the present level of operational capacity of highway infrastructures in Ontario. Therefore, there is a need of recommendations for revising the existing design standards to include the

anticipated climate change effects in order to avoid an increase in the risk of “failure” of highway infrastructures in Ontario.

# Introduction

---

## **A. STATEMENT OF THE PROBLEM**

Recent scientific studies indicate that the mean annual global surface temperature has increased by about 0.3°C to 0.6°C since the late 19th century, and a report by the Intergovernmental Panel on Climate Change (IPCC) estimates a further increase between 1°C and 3.5°C over the next 100 years (IPCC, 1995, 2001). As a result, the hydrologic cycle is expected to become more active and intensify, leading to an increase in the precipitation intensity and the number of severe storm events (IPCC, 1995, 2001). This has been corroborated by the analysis of Canadian daily precipitation time series from 1940 to 1998 which shows that the fraction of annual precipitation falling in heavy events increased by about 3% in average (Mekis and Hogg, 1999). Further recent study has shown that global climate change is associated with increasing extreme storm events at regional and local scale throughout the northern hemisphere (Folland et al., 2001). Climate change that produces an increase in the intensity of precipitation will increase the magnitude of the design discharge and that would most likely result in adverse effects on existing drainage facilities. This raises an important question: should new drainage design standards be established in order to include the effects of the anticipated climate change?

## **B. BACKGROUND**

Human activities, primarily the burning of fossil fuels and changes in land cover and use, are nowadays believed to be increasing the atmospheric concentrations of greenhouse gases. This alters energy balances and tends to warm the atmosphere which results in climate change. These changes in global climate appear to most severely affect the mid and high latitudes of the Northern Hemisphere, where temperatures have been noticeably getting warmer since 1970s (IPCC, 2001). Such changes in climate will also have significant impact on local and regional hydrological regimes, which will in turn affect ecological, social and economical systems.

Global Circulation Models (GCMs) are nowadays being used to simulate the present climate and project future climate scenarios with forcing by greenhouse gases and aerosols. Such models predict on the global scale, a possible increase of 8% and 14% in 20-year return period of daily precipitation by 2050s and 2090s respectively (Kharin and Zwiers, 2000). Though the spatial resolution of GCMs remains quite coarse, daily precipitation series corresponding to future climate scenarios can be derived at a regional or local scale from GCM outputs using the so called 'downscaling techniques'. Such

recent study in Northern Quebec suggested an average increase in daily total precipitation of about 15% to 30% in the next 100 years (Coulibaly and Dibike, 2004). Such an increase in total precipitation also implies a corresponding increase in the intensity of shorter time scale storm events.

A recent workshop on the 'Impact of Climate Change on Transportation in Canada' organized by Transport Canada has investigated the reality of global climate change and stressed that the impacts of such a change on transportation infrastructure in Canada have to be investigated further (Marbek, 2003). The report also indicated that in some regions in Canada, an apparent increase in the number of extreme events with several 100-year storms has been witnessed in the span of a few decades. It was further noted that such an increase in the frequency of storm events will affect transportation operation and public safety unless climate change adaptations are to be integrated into routine government planning based on the available scientific information. The report also emphasized the importance of further climate change impact research focusing on specific regions and high risk areas.

Under normal circumstances, highway drainage structures which remove storm water from the roadway and convey surface and stream waters originating upstream of the highway to the downstream side, are designed to accomplish these functions without causing objectionable backwater, excessive velocities, erosion or unduly affecting traffic safety. That means, one of the goals in highway drainage design is to allow natural drainage, insofar as practical, and prevents the retention of water by the highway. Therefore, such design must consider the probability of flooding and provides protection which is commensurate with the importance of the highway, the potential for property damage, and traffic safety. By applying analytical principles and methods, it is possible to obtain such peak discharge estimates which are functionally acceptable for the design of the highway drainage structures and other features. Traditionally, the level of assurance for such protection has been specified in terms of peak flow rate during the passage of a severe storm event or a flood associated with a frequency of occurrence, such as a 20-year storm, or a 50-year flood, etc.

Recent studies in different regions have shown that climate change that produces an increase in the intensity of precipitation will most likely result in adverse effects on drainage systems (Denault et al., 2002; Kije Sipi Ltd, 2001). Nevertheless, drainage systems have always been designed on the premise that the climate is not changing and that historical climate data can be effectively used to predict future drainage design requirements. Therefore, there is a need to assess whether the actual drainage design guidelines should improved in order to include potential climate change effects. Since Ontario highways are amongst the critical transportation infrastructures in the province to which the impact of climate change needs to be thoroughly investigated, the proposed research aims to provide a comprehensive investigation of possible climate change impacts on the drainage facilities of selected major highways in Ontario.

## **C. RESEARCH OBJECTIVES**

Although many organizations are undertaking various researches on climate change, there is no well establish methodologies to relate the anticipated changes in weather to the impact of such changes on the performance of hydraulic structures such as bridges, culverts and sewer systems. The ultimate goal of this research is to fill this gap and provides a robust method for assessing possible climate change impact on the design standards of future drainage facilities. Therefore, this research will first assess the state of research and propose appropriate methodologies on how to apply the scientific information of climate change available to date on the design of future highway drainage infrastructure in Ontario. The specific objectives of the study can be summarized as follows:

- Collect station records of daily precipitation in the selected study areas, and perform trend analysis on maximum daily precipitation.
- Identify the climate change scenario that is the most likely to reflect the future climate trend in Ontario, and obtain Global Circulation Models (GCMs) simulation outputs corresponding to the selected future climate scenario.
- Use spatial downscaling technique to downscale the GCM outputs and generate future precipitation series representing the local conditions of the areas to be investigated. Perform time series analysis on these predicted precipitation data to assess possible trend in the frequency and magnitude of storm events in the selected study regions.
- Identify the consequences of the anticipated changes in the intensity and frequency of storm events of the future climate on the existing drainage facilities, and recommend improvement in the existing design standards so as to maintain the present level of operational capability and avoid an increase in the risk of “failure”.

Two study areas of interest have been selected: The Grand River Region in southern Ontario, and the Kenora and Rainy River Region in northwestern Ontario. The selected study areas cover the major national and provincial highways.

## **D. ORGANIZATION OF THE REPORT**

Chapter 2 presents the study areas and the data used in this study.

Chapter 3 describes the non-parametric trend test used, and provides the trend analysis results for the historical precipitation data. Further precipitation trend analysis based on IDF curves is also provided.

Chapter 4 introduces the statistical downscaling model, and presents the downscaling results for the current and future climate condition.

Chapter 5 provides the comparison of IDF curves for the current and future periods at each station. This includes the estimates of changes in the precipitation intensity between the current and the future climate condition.

Chapter 6 presents the design experiment using the rational method, and demonstrates the potential changes in sewer pipe diameter in order to withstand future storm events.

Chapter 7 presents the summary and conclusions from this research project.

Chapter 8 provides the final recommendations of the research.

# Study Areas and Data Used

## A. STUDY AREAS

The study areas selected in this research project for the application of downscaling method and evaluation of the impact of climate change on the drainage design standards are the Grand River Region in southern Ontario and the Kenora and Rainy River Region in northwestern Ontario (Figure 1).



Figure 1 - Location Map of Study Areas in Ontario



The Kenora and Rainy River region (Figure 3) is located in Northwestern Ontario, and covers the municipalities of Kenora, Rainy River and Fort Frances. It extends from 93.4° to 94.7° West and 48.6° to 50° North. The Trans-Canada Highway, the Hwy 17, the Hwy 71, and other important municipal roads along with many drainage infrastructures are present in this region.

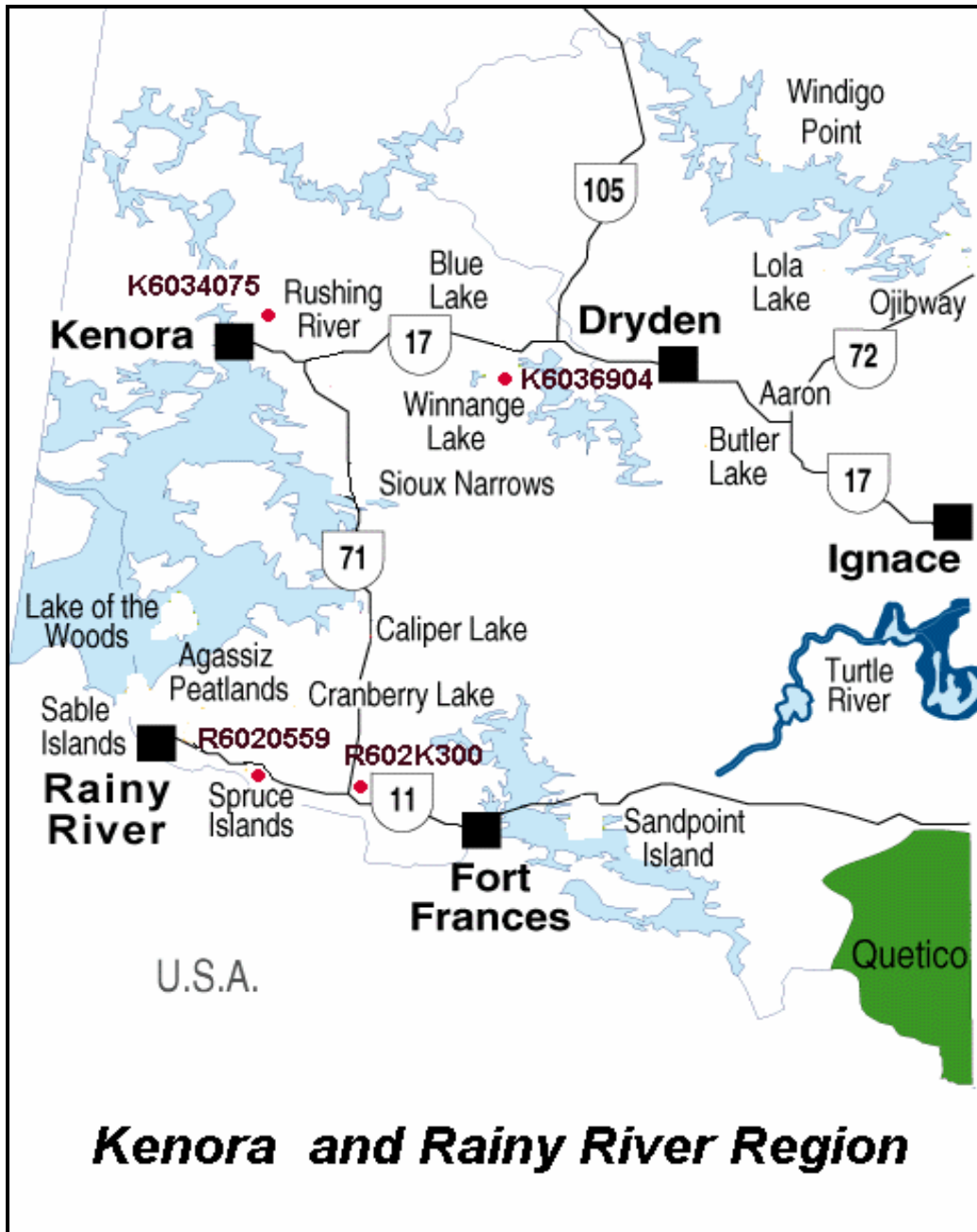


Figure 3 - Location Map of Weather Stations in the Kenora and Rainy River Region

## **B. DATA COLLECTION**

In this research project, observed daily data of large-scale predictor variables representing the current climate condition is derived from the national centre for environmental prediction (NCEP) reanalysis data set (Kistler et al., 2001). The Canadian Centre for Climate Modeling and Analysis (CCCma) provides GCM daily data of a number of surface and atmospheric variables for the time period 1961-2100. The data is extracted from an ensemble of three 111-year simulations with the Canadian Global Circulation Model-2 (CGCM2) using the IPCC SRES B2 scenario. The B2 scenario is one of the most conservative scenarios, which produces less warming than the IPCC “IS92a” scenario used in various impact studies (Morrison et al., 2002; Dibike and Coulibaly, 2005). The corresponding data for the Grand River Region and the Kenora and Rainy River Region is extracted from the CGCM2 outputs at the grid point 42.67°N, 78.75°W and 50.10°N, 93.75°W respectively. Those are the closest grid points to the study areas where CGCM2 outputs are available. The data is divided into four distinct periods, namely, the current (1961- 2000), the 2020s (2010-2039), the 2050s (2040-2069) and the 2080s (2070-2099) to facilitate trend analysis.

Moreover, observed (historical) precipitation records at eight meteorological stations in the two study areas are collected (Table 1). Four stations are located in the Grand River Region (Figure 2) and the four other stations are located in the Kenora and Rainy River Region (Figure 3). The observed and downscaled precipitation data at these eight stations are used in the analysis of the impact of the anticipated climate change on future design standards of drainage infrastructure.

**Table 1 - Selected Meteorological Stations**

	Station Name	Station Number	Time Period	Elevation (m)	Coordinates	
					Longitude (W)	Latitude (N)
Grand River Region	Brantford	G6140954	1961-2000	196	80°14'	43°08'
	Stratford	G6148105	1960-2000	354	81°	43°22'
	Glen Allan	G6142803	1959-2000	404	80°43'	43°41'
	Woodstock	G6149625	1961-2000	282	80°46'	43°08'
Kenora and Rainy River Region	Kenora A	K6034075	1939-2000	406	94°22'	49°47'
	Rawson Lake	K6036904	1970-2000	358	93°43'	49°39'
	Barwick	R6020559	1979-2000	335	93°58'	48°38'
	Emo Radbourne	R602K300	1979-2000	350	93°50'	48°41'

---

# Precipitation Trend Analysis

---

## A. MANN-KENDALL TREND TEST

Trend testing for hydro-meteorological variables such as precipitation, temperature and streamflow has been of particular interest to hydrologists and researchers for several decades. A comprehensive review of statistical approaches used for trend analysis of water resources time series is provided by Helsel and Hirsch (1992). More recent studies indicate that the most widely used method is the non-parametric Mann-Kendall trend test (Douglas et al., 2000; Zhang et al., 2001; Kahya and Kalayci, 2004). Mann (1945) originally derived the test and Kendall (1975) subsequently derived the test statistic commonly known as the Kendall's tau statistic. This test is a non-parametric test that means it does not assume any priority distribution of the data, and is therefore robust in comparison to parametric tests. It was found to be an excellent tool for trend detection in different applications (Hirsch et al., 1982; Gan 1992; Yue et al., 2002; Burn and Hag-Elnur, 2002).

To determine if there is a trend in the precipitation data for each station in the Grand River Region and the Kenora and Rainy River Region, the Mann-Kendall trend test is used. The null hypothesis ( $H_0$ ) means no trend, while the alternative ( $H_1$ ) is that there is a trend. The test first ranks all observations by time series. Then the difference between each successive value is calculated, and the sum of the signs of those differences is evaluated as the Mann-Kendall statistic  $S$  (Kendall, 1975) as follows:

$$S = \sum_{i=1}^{n-1} \sum_{j=i+1}^n \text{sgn}(x_j - x_i) \quad (\text{Eq. 1})$$

where the  $x_j$  are the sequential data values,  $n$  is the length of the data set, and

$$\text{sgn}(\theta) = \begin{cases} 1 & \text{if } \theta > 0 \\ 0 & \text{if } \theta = 0 \\ -1 & \text{if } \theta < 0 \end{cases} \quad \text{where } \theta = (x_j - x_i) \quad (\text{Eq. 2})$$

This process is repeated iteratively until all successive differences have been evaluated. The Mann-Kendall statistic  $S$  is then compared to a critical value. If it exceeds that value, there is an upward trend when  $S > 0$ , or a downward trend when  $S < 0$ . The sample size is important in determining the critical value for  $S$ . Mann and Kendall have documented

that when  $n \geq 8$ , the statistic  $S$  is approximately normally distributed with the mean and the variance given by

$$E(S) = 0 \quad (\text{Eq. 3})$$

$$V(S) = \frac{n(n-1)(2n+5) - \sum_{i=1}^n t_i i(i-1)(2i+5)}{18} \quad (\text{Eq. 4})$$

where  $t_i$  is the number of ties of extent  $i$  (i.e. a dataset with two tied values would have one tie of extent two or  $i = 2$  and  $t_2 = 1$ ). The standardized Mann-Kendall test statistic  $Z_{MK}$  is computed by

$$Z_{MK} = \begin{cases} \frac{S-1}{\sqrt{\text{Var}(S)}} & S > 0 \\ 0 & S = 0 \\ \frac{S+1}{\sqrt{\text{Var}(S)}} & S < 0 \end{cases} \quad (\text{Eq. 5})$$

$Z_{MK}$  follows a standard normal distribution with mean of zero and variance of one. The positive (or negative) value of  $Z$  indicates an upward (or downward) trend. If no trend exists, the  $Z$ -score represents a standard normal distribution. Alternatively,  $Z$  has a positive or negative value. Significance levels ( $p$ -values) for each trend test can be obtained from

$$p = 0.5 - \Phi(|Z_{MK}|) \quad (\text{Eq. 6})$$

where  $\Phi( )$  denotes the cumulative distribution function (cdf) of a standard normal variate. In general, for  $p$ -value small enough, the trend is unlikely to be caused by random sampling. At the significance level of 0.05, if  $p \leq 0.05$ , then the existing trend is considered to be statistically significant (Yue et al., 2002).

## B. PRECIPITATION TREND ANALYSIS

The annual maximum daily precipitation refers to the observed maximum daily precipitation value for each year. The Mann-Kendall trend test is applied to this data series. In the Grand River Region, three of the stations (G6140954, G6148105 and G6149625) show increasing trend at non-significance levels of  $p = 0.65$ ,  $p = 0.44$  and  $p = 0.68$  respectively, while one station (G6142803) shows a decreasing trend at non-significance level  $p = 0.63$ . The latter may be related to local geographical effect (e.g. topography, altitude, vegetation, ...).

In the Kenora and Rainy River Region all the four stations (K6034075, K6036904, R6020559 and R602k300) show increasing trend. These results are shown in Figure A1 to Figure A8 (in the Appendix) for each station. The trend analysis results for the annual maximum daily precipitation data are also summarized in Table 2. Further precipitation trend analysis is provided in section C using the intensity-duration-frequency (IDF) curves.

**Table 2 - Summary of Trend Analysis Results**

	Station Name	Annual Maximum Daily Precipitation
Grand River Region	G6140954 (Brantford)	Increased and Insignificant ( $p= 0.65$ )
	G6148105 (Stratford)	Increased and Insignificant ( $p= 0.44$ )
	G6142803 (Glen Allan)	Decreased and Insignificant ( $p=0.63$ )
	G6149625 (Woodstock)	Increased and Insignificant ( $p= 0.68$ )
Kenora and Rainy River Region	K6034075 (Kenora A)	Increased and Significant ( $p= 0.006$ )
	K6036904 (Rawson Lake)	Increased and Insignificant ( $p= 0.1$ )
	R6020559 (Barwick)	Increased and Insignificant ( $p= 0.31$ )
	R602K300 (Emo Radbourne)	Increased and Insignificant ( $p= 0.21$ )

### C. IDENTIFYING TRENDS IN OBSERVED PRECIPITATION USING IDF CURVES

Rainfall intensity-duration-frequency (IDF) curves are derived from statistical analysis of rainfall records over a period of time. Each curve represents the intensity-time relationship for a certain return period from a series of storms. These curves are said to represent storms specific return frequency. Development of intensity-duration-frequency curves is a very important step in highway drainage design. In general, IDF curves are made available for a specific site. The information is usually presented as a graph with duration plotted on the horizontal axis, intensity on the vertical axis, and a series of curves, one for each design return period. The intensity represents the rate of precipitation, given in, depth per unit time (mm/hr or in/hr). Figure 4 is a typical example of an IDF curve for Chicago, Illinois, U.S.A (Chow et al., 1988).

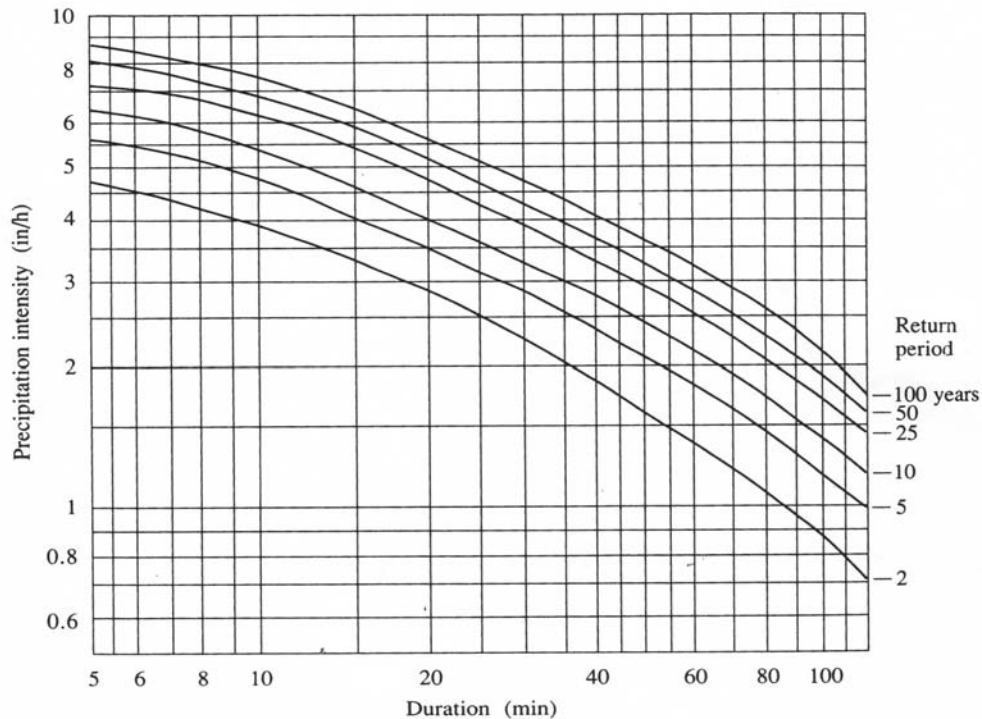


**Figure 4 - Intensity-Duration-Frequency (IDF) Curves of Maximum Rainfall in Chicago, Illinois.**

Frequency is expressed in terms of return period,  $T$ , which is the average length of time between precipitation events that equal to or exceed a given magnitude. When local rainfall data are available, IDF curves are developed using statistical frequency analysis. For each of the selected durations, the annual maximum rainfall depths are extracted from historical rainfall records, and then frequency analysis for different durations is applied to the annual maximum precipitation.

## 1. CONSTRUCTION OF IDF CURVES FOR EACH STATION

In order to assess whether there is a change in the frequency of the extreme precipitation events in the recent past years, we divided the historical daily precipitation data at each recording station in the Grand River Region (G6140954, G6148105, G6142803 and G6149625) into two periods and construct IDF curves for each time period. For example, at the station G6140954, the data from 1961 to 1980 is the first period and the second period is from 1981 to 2000. Several equations have been developed to express rainfall intensity in terms of storm duration  $t_d$  (Chow et al., 1988). For areas where limited precipitation data are available, precipitation intensity can be estimated by:

$$i = \frac{a}{(t_d + b)^m} \quad (\text{Eq. 7})$$

where  $i$  is the average rainfall intensity (mm/hr) for a given duration  $t_d$  (hr);  $a$ ,  $b$ , and  $m$  are empirical coefficients that are determined through statistical analysis of local rainfall data. Here the construction procedure of IDF curves is expressed in the following. Given that for each meteorological station, only daily rainfall are available, there is a need to convert the daily rainfall to shorter-duration (i.e. less than 24hr) rainfall (e.g. X-hr rainfall, for  $X = 18\text{hr}, 12\text{hr}, \dots, 5 \text{ min.}$ ). This requires a conversion technique (namely “transformation factor”) initially introduced by Hershfield (1961), and adapted subsequently by Huff and Angel (1989). The transformation factor is an average value that is site-specific, and based on available raingage data. It can vary between storms, however this results in small errors when applied to a large sample of storms (Huff and Angel, 1989). The transformation factor for 1-day to 24-hr rainfall was found to be 1.13 (Huff and Angel, 1989, 1992) using rainfall records from Illinois stations. For storm durations less than 24hr, the average ratios of X-hr/24-hr rainfall was used. The derived rainfall ratios for rain of durations ranging from 5 minutes to 18 hours are shown in Table-3 for the Illinois stations. This ratio approach of obtaining shorter-duration (e.g. less than 24hr) rainfall can be applied in any area where average ratios of X-hr/24-hr rainfall are available. In our study area, the average ratios (Table - 4) are obtained from the Hydrological Atlas of Canada (1978). Short-duration rainfall permits the frequency analysis of rain events of less than 24hr. This is particularly important for hydraulic structures design. Afterwards, the Gumbel distribution is used for the frequency analysis,

and precipitation amount for events having 2-yr, 5-yr, 10-yr, 20-yr, 50-yr and 100-yr return periods are obtained. More interestingly this includes precipitation amount for shorter-durations (ranging from 5 minutes to 18-hr).

**Table 3 - Average Ratio of X-hour/24-hour Rainfall for Illinois**

Rainfall duration $T_d$ (hours)	Ratio (X-hour/24-Hour)
18	0.94
12	0.87
6	0.75
3	0.64
2	0.58
1	0.47
0.50 (30 min.)	0.37
0.25 (15 min.)	0.27
0.17 (10 min.)	0.21
0.08 (5 min.)	0.12

**Table 4 - Average Ratio of X-Hour/24-Hour Rainfall for Ontario**

Rainfall duration $T_d$ (hours)	Ratio (X-hour/24-Hour)
18	0.91
12	0.82
6	0.73
3	0.64
2	0.56
1	0.45
0.50 (30 min.)	0.38
0.25 (15 min.)	0.29
0.17 (10 min.)	0.22
0.08 (5 min.)	0.12

## 2. COMPARISON OF THE IDF CURVES FOR EACH STATION

Now we can construct the IDF curves for each station in the Grand River Region and compare the IDF curves of the two periods to identify possible trends in the historical precipitation data.

### a. Station G6140954 (Brantford)

The IDF curves (Figure A9 and Figure A10 in Appendix) are for the two periods 1961-1980 and 1981-2000 respectively. It appears from the results in Table A1 and Table A2 (in Appendix) that for the same duration and return periods, the precipitation intensity has increased from the 1961-1980 to the 1981-2000 time period.

A comparison of the 24-hour duration precipitation at the station G6140954 is shown in Table 5 and Figure 5 for the two time periods 1961-1980 and 1981-2000. The 4.7% increase in the 2-year precipitation and the 20.1 % increase in the 100-year precipitation between the two periods show how the intensity of observed precipitation increased in the recent years.

**Table 5 - Observed 24-hour Precipitation (mm) Comparison for 1961-1980 and 1981-2000 at Station G6140954**

Return period (Years)	2	5	10	20	50	100
1961-1980	50.7	62.1	69.7	77.0	86.4	93.5
1981-2000	53.0	68.9	79.4	89.5	102.5	112.3
Change (%)	4.7	10.9	13.9	16.2	18.6	20.1

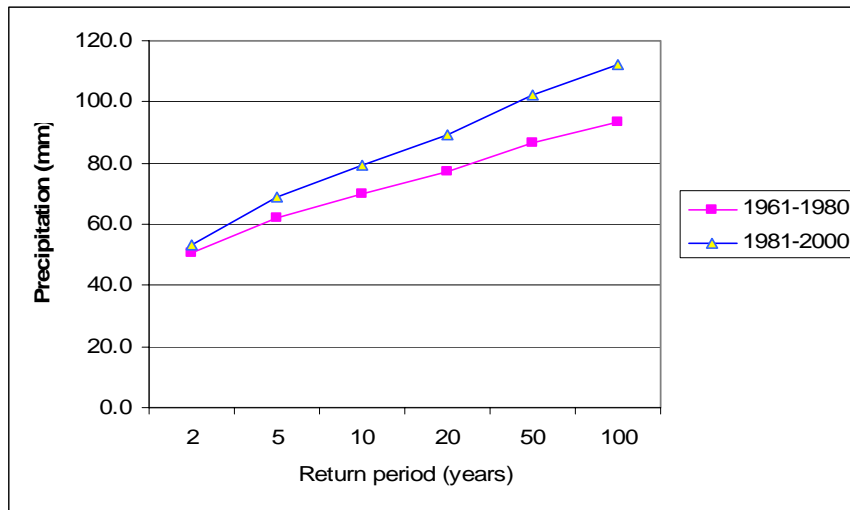


**Figure 5 - Comparison of 24-Hour Precipitation Between 1961-1980 and 1981-2000 at Station G6140954**

**b. Station G6148105 (Stratford)**

The IDF curves (Figure A11 and Figure A12 in Appendix) are constructed for the two periods: 1961-1980 and 1981-2000 at the station G6148105. From the results in Table A3 and Table A4 (in Appendix), it appears that for the same duration and return periods, the precipitation intensity has significantly increased between the 1961-1980 and 1981-2000 time periods.

The comparative results of the observed 24-hour precipitation for the two periods (1961-1980 and 1981-2000) are presented in Table 6 and Figure 6. The results clearly highlight how the observed precipitation intensity has increased in the last two decades (1981-2000). Specifically, the increase ranges from of 3% for the 2-year precipitation to 66.1% for the 100-year precipitation between the two time periods.

**Table 6 - Observed 24-hour Precipitation (mm) Comparison for 1961-1980 and 1981-2000 at Station G6148105**

Return period (Years)	2	5	10	20	50	100
1961-1980	54.1	66.6	74.8	82.7	93.0	100.6
1981-2000	55.7	85.5	105.3	124.2	148.8	167.1
Change (%)	3.0	28.5	40.7	50.2	60.0	66.1

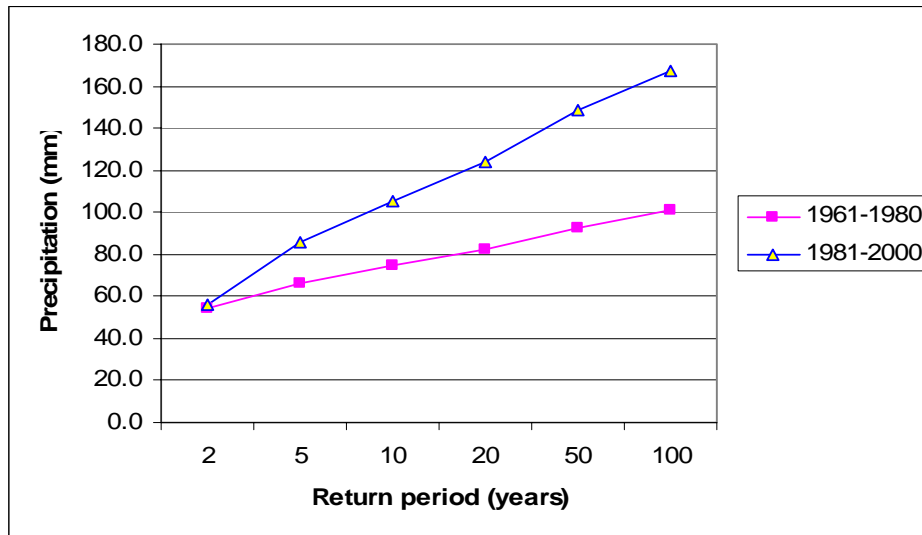


**Figure 6 - Comparison of 24-Hour Precipitation Between 1961-1980 and 1981-2000 at Station G6148105**

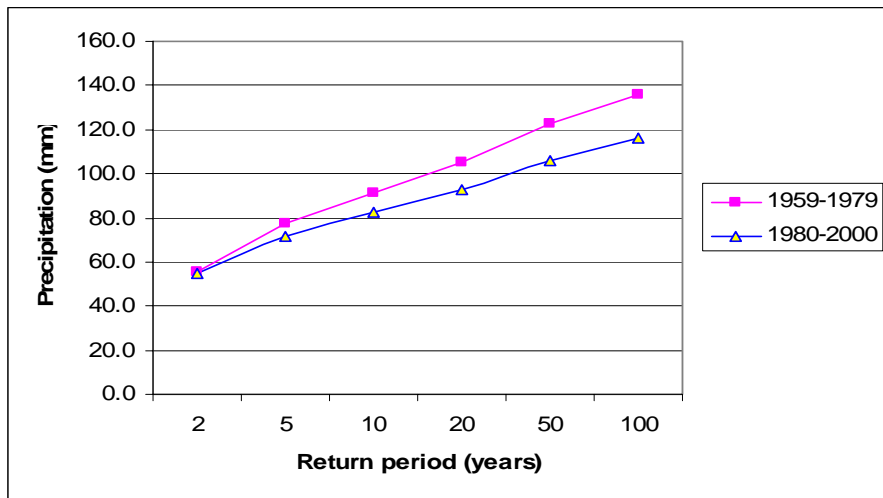
**c. Station G6142803 (Glen allen)**

The IDF curves (Figure A13 and Figure A14) are for the two periods: 1959-1979 and 1980-2000 at the station G6142803. Obviously, from Table A5 and Table A6, it appears that the precipitation intensity has decreased between the 1959-1979 and 1980-2000 time periods for the same duration and return periods. This is consistent with the trend analysis results shown previously for that station.

The comparison of observed 24-hour precipitation (Table 7 and Figure 7) for the two periods 1959-1979 and 1980-2000 shows how the precipitation intensity decreased at station G6142803. Specifically, the decrease ranges from 1% for the 2-year precipitation to 14.5 % for the 100-year precipitation.

**Table 7 - Observed 24-Hour Precipitation (mm) Comparison for 1959-1979 and 1980-2000 at Station G6142803**

Return period (Years)	2	5	10	20	50	100
1961-1980	55.7	77.1	91.3	104.9	122.5	135.7
1981-2000	55.1	71.4	82.2	92.6	106.0	116.0
Change (%)	-1.0	-7.4	-9.9	-11.7	-13.5	-14.5



**Figure– 7 Comparison of 24-Hour Precipitation Between 1959-1979 and 1980-2000 at Station G6142803**

**d. Station G6149625 (Woodstock)**

The IDF curves (Figure A15 and Figure A16) are for the two periods: 1961-1980 and 1981-2000 at the station G6149625. From the results in Table A7 and Table A8, it appears that for the same duration and return periods, the precipitation intensity has significantly increased from the 1961-1980 to 1981-2000 time periods.

The comparative results of the observed 24-hour precipitation for the two periods (1961-1980 and 1981-2000) are presented in Table 8 and Figure 8. The results confirm that the observed precipitation intensity has increased in the last two decades (1981-2000). There is an increase of 18.6 % for the 2-year precipitation and 59.7 % for the 100-year precipitation between the two time periods.

**Table 8 - Observed 24-Hour Precipitation (mm) Comparison for 1961-1980 and 1981-2000 at Station G6149625**

Return period (Years)	2	5	10	20	50	100
1961-1980	54.1	65.8	73.5	80.9	90.5	97.7
1981-2000	64.2	88.8	105.1	120.7	140.9	156.0
Change (%)	18.6	34.9	42.9	49.1	55.7	59.7

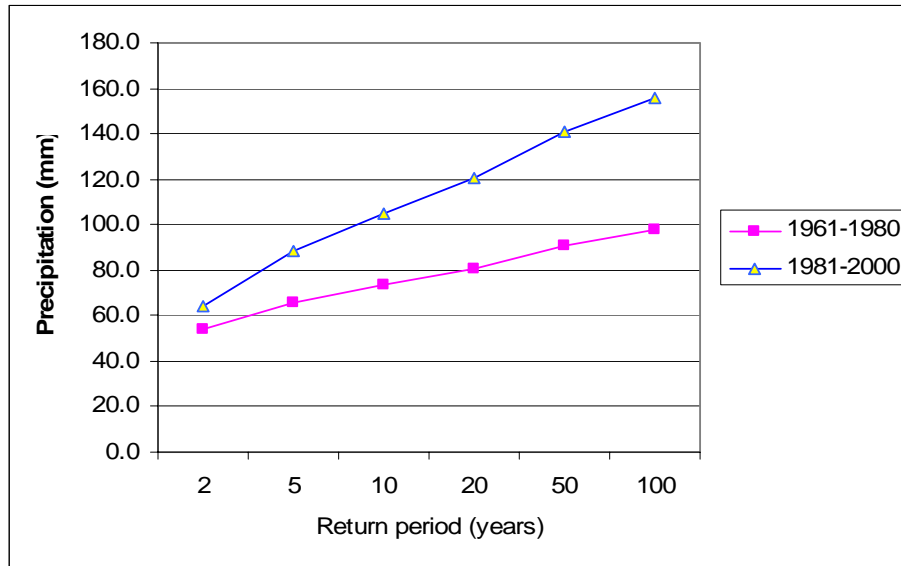


**Figure 8 - Comparison of 24-Hour Precipitation Between 1961-1980 and 1981-2000 at Station G6149625**

Overall, the above Tables and Figures clearly illustrate the trends in the IDF curves for observed precipitation at each station. While the stations G6140954, G6148105 and G6149625 show a significant increase in the precipitation intensity in the recent time period (1980s-2000), a decreasing trend is observed only at one station (G6142803). In addition, we also noticed that the trends in the IDF curves at all the stations are consistent with the trends in annual maximum daily precipitation shown in earlier section B

## **D. SUMMARY OF TREND ANALYSIS RESULTS**

By using the Mann-Kendall trend test and the IDF curves, it is shown that in general, there are increasing trends in the magnitude and intensity of observed precipitation data in both the Grand River Region and Kenora and Rainy River Region. The annual maximum daily precipitation exhibits increasing trends for three of the four stations (G6140954, G6148105 and G6149625) in the Grand River Region, and for all the four stations in the Kenora and Rainy River Region (K6034075, K6036904, R6020559 and R602k300). Only one station (G6142803) shows a decreasing trend in the annual maximum daily precipitation, which appears to be related to local geographic effect. In addition, the IDF curves for all the stations show similar trends with that of the annual maximum daily precipitation. For almost all the eight stations, there is a significant increase in the 24-hour precipitation intensity in the last two decades (1980s-2000).

Trends in precipitation series can be significantly different within the same region while based on station records. Thus all available historical records should be considered for the trend analysis to account for the spatial variability. Meanwhile, the increasing and decreasing trends in observed precipitation intensity within the same region highlight the possible variability of the impact of the anticipated climate change at local or regional scale.

# Downscaling Daily Precipitation

---

## A. STATISTICAL DOWNSCALING MODEL

Global Circulation Models (GCMs) are generally not designed for local climate change impact studies and their spatial resolution remains quite coarse, in the order of 300 x 300 km, and at that scale, the regional and local details of the climate which are influenced by spatial heterogeneities in the regional physiography are lost. GCMs are therefore inherently unable to represent local subgrid-scale features and dynamics, such as local topographical features and convective cloud processes. Therefore, there is the need to convert the GCM outputs into at least a reliable daily precipitation series at the scale of the area to which the impact is going to be investigated. The methods used to convert GCM outputs into local meteorological variables required for reliable hydrological modeling are usually referred to as 'downscaling' techniques. A Statistical Down-Scaling Model (SDSM) is employed in this study. The selected downscaling method has already been thoroughly tested and compared for daily rainfall scenarios constructions for flood regime assessment in the Saguenay basin (Coulibaly and Dibike, 2005). The downscaling model is calibrated and validated using the historical precipitation (as predictand) and the observed reanalysis daily data of large-scale predictor variables representing the current climate condition. The calibrated model is then used to downscale the large scale atmospheric variables derived from GCM simulations and estimate the corresponding daily precipitation values for each study area.

The Statistical Down-Scaling Model (SDSM) is a multiple linear regression based downscaling method that is widely used for spatial downscaling of daily meteorological variables such as precipitation and temperature by identifying predictor-predictand relationships using multiple linear regression technique. The predictor variables provide daily information concerning the large-scale state of the atmosphere, whilst the predictand describes conditions at the site scale. The SDSM reduces the task of statistically downscaling daily weather series into a number of discrete processes as follows (Wilby et al., 2002):

1. Preliminary screening of potential downscaling predictor variables - identifies those large-scale predictor variables which are significantly correlated with observed station (predictand) data.
2. Assembly and calibration of statistical downscaling model(s) - the large-scale predictor variables identified in (1) are used in the determination of multiple linear regression relationships between these variables and the local station data. Statistical models may be built on a monthly, seasonal or annual basis.

Information regarding the amount of variance explained by the model(s) and the standard error is given in order to determine the viability of spatial downscaling for the variable and site in question.

3. Synthesis of ensembles of current weather data using observed predictor variables - once statistical downscaling models have been determined they can be verified by using an independent data set of observed predictors. The stochastic component of SDSM allows the generation of up to 100 ensembles of data which have the same statistical characteristics but which vary on a day-to-day basis.
4. Generation of ensembles of future weather data using GCM-derived predictor variables - provision of the appropriate GCM-derived predictor variables allows the generation of ensembles of future weather data by using the statistical relationships established in (2).
5. Diagnostic testing/analysis of observed data and climate change scenarios - it is possible to calculate the statistical characteristics of both the observed and synthetic data in order for easy comparison and thus determination of the effect of spatial downscaling.

Although the software provides a procedure for selecting predictor variables, the final decision should be based on physically sensible linkage between the large-scale forcing and local meteorological response. Therefore, the best practice demands the rigorous evaluation of candidate predictor-predictand relationships prior to downscaling (Wilby et al., 2002).

From the forty years of data representing the current climate, the first 30 years (1961-1990) are considered for calibrating the regression models while the remaining ten years of data (1991-2000) are used to validate those models. Some of the SDSM setup parameters such as event threshold, bias correction and variance inflation were adjusted during calibration to get the best statistical agreement between observed and simulated climate variables.

For SDSM, selecting the most relevant predictor variables is the first and important task in the downscaling process. The task of screening the most relevant predictor variables is achieved with linear correlation analysis and scatter plots (between the predictors and the predictand variables). Observed daily data of large-scale predictor variables representing the current climate condition (1961 – 2000) derived from the NCEP reanalysis data set is used to investigate the percentage of variance explained by each predictand-predictor pairs. Moreover, the strength of individual predictors varies on a month by month basis; therefore, the most appropriate combination of predictors has to be chosen by looking at the analysis output of all the twelve months. However, the final choice is made by considering whether the identified variables and relationships are physically sensible for the particular experiment and study site. The predictor variables identified for each downscaling experiment conducted in this study are summarized in Table 9. The result

shows that the same set of large-scale predictors is needed to predict the local predictand variable at each station.

**Table 9 - Summary of Selected Large-Scale Predictor Variables for the Downscaling of Daily Precipitation**

	Predictor variable	Description
Predictors	p_v	Meridional velocity component near surface
	p8_v	Meridional velocity component at 850 hPa height
	p8zh	Divergence at 850 hPa height
	s500	Specific humidity at 500 hPa height
	s850	Specific humidity at 850 hPa height
	shum	Near surface specific humidity
	temp	Mean temperature
	p500	500 hPa geopotential height

## **B. DOWNCALING MODEL VALIDATION RESULTS**

During the calibration of precipitation downscaling model, the maximum daily precipitation and daily precipitation variability for each month constituted the performance criteria. Figure 9 and Figure 10 show the model performance during the validation period. The graphs show a good agreement between the observed and the simulated values for the maximum daily precipitation and the daily precipitation variability in terms of standard deviation. Although the accuracy of the downscaling results varies from month to month and also from one station to another, overall, the downscaled maximum precipitation values are very good as compared to the raw CGCM2 simulated precipitation. This will be highlighted later herein.

To further assess the accuracy of the downscaled results as compared to the observed values, root mean square error (RMSE) statistics of the validation results are presented in Table 10 for all the stations. For two of the stations (G6140954 and G6149625) in the Grand River Region and for two stations (K6036904, and R6020559) in the Kenora and Rainy River Region, the downscaled results appear very good based on the very low RMSE (less than 22% in average), while for the remaining stations, the downscaling results are good (average RMSE less than 39%). Therefore the downscaling model appears an appropriate model for generating future precipitation series at each of the station.

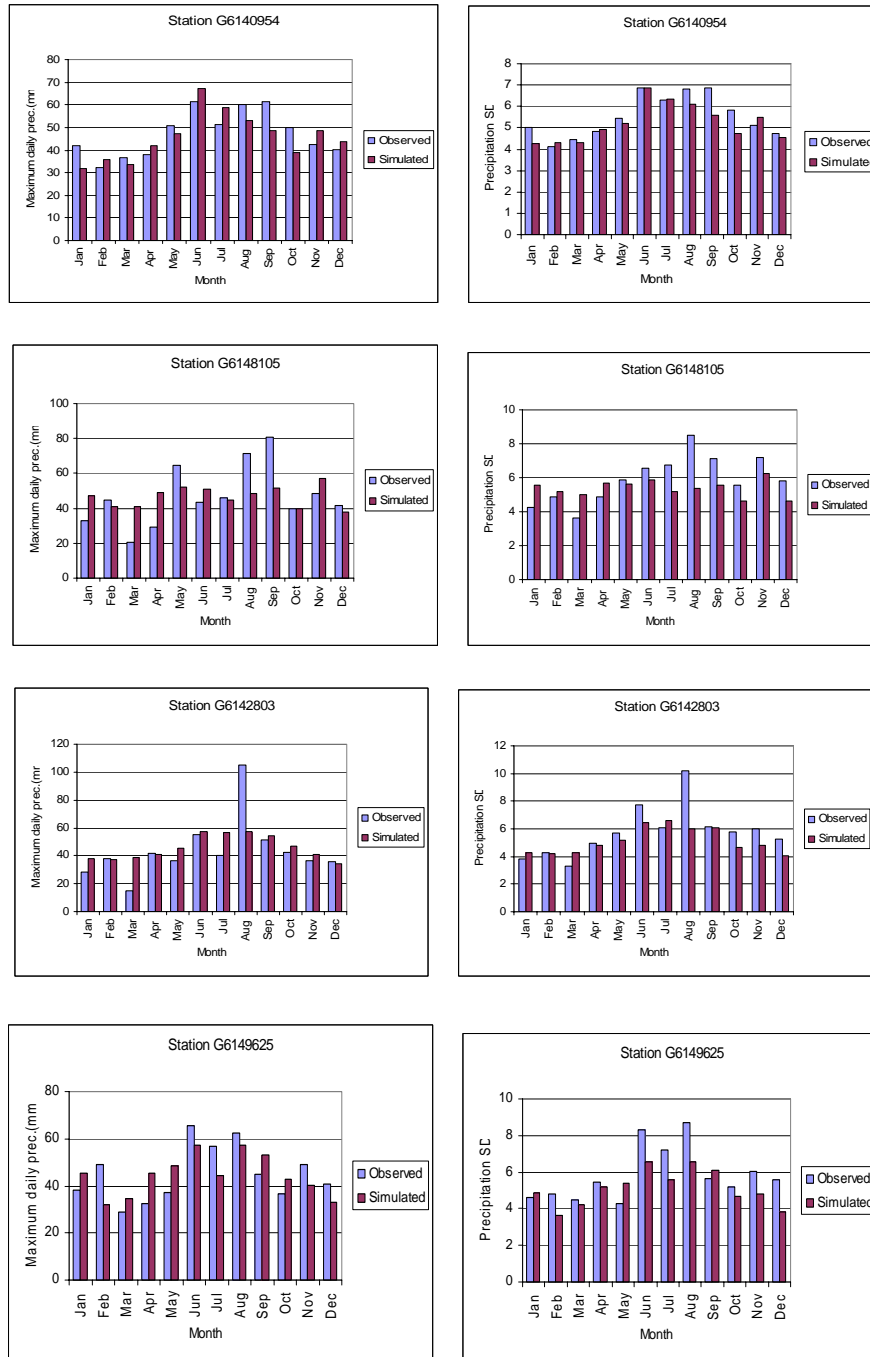


**Figure 9 - SDSM Validation Results of Downscaling Daily Precipitation in the Grand River Region**

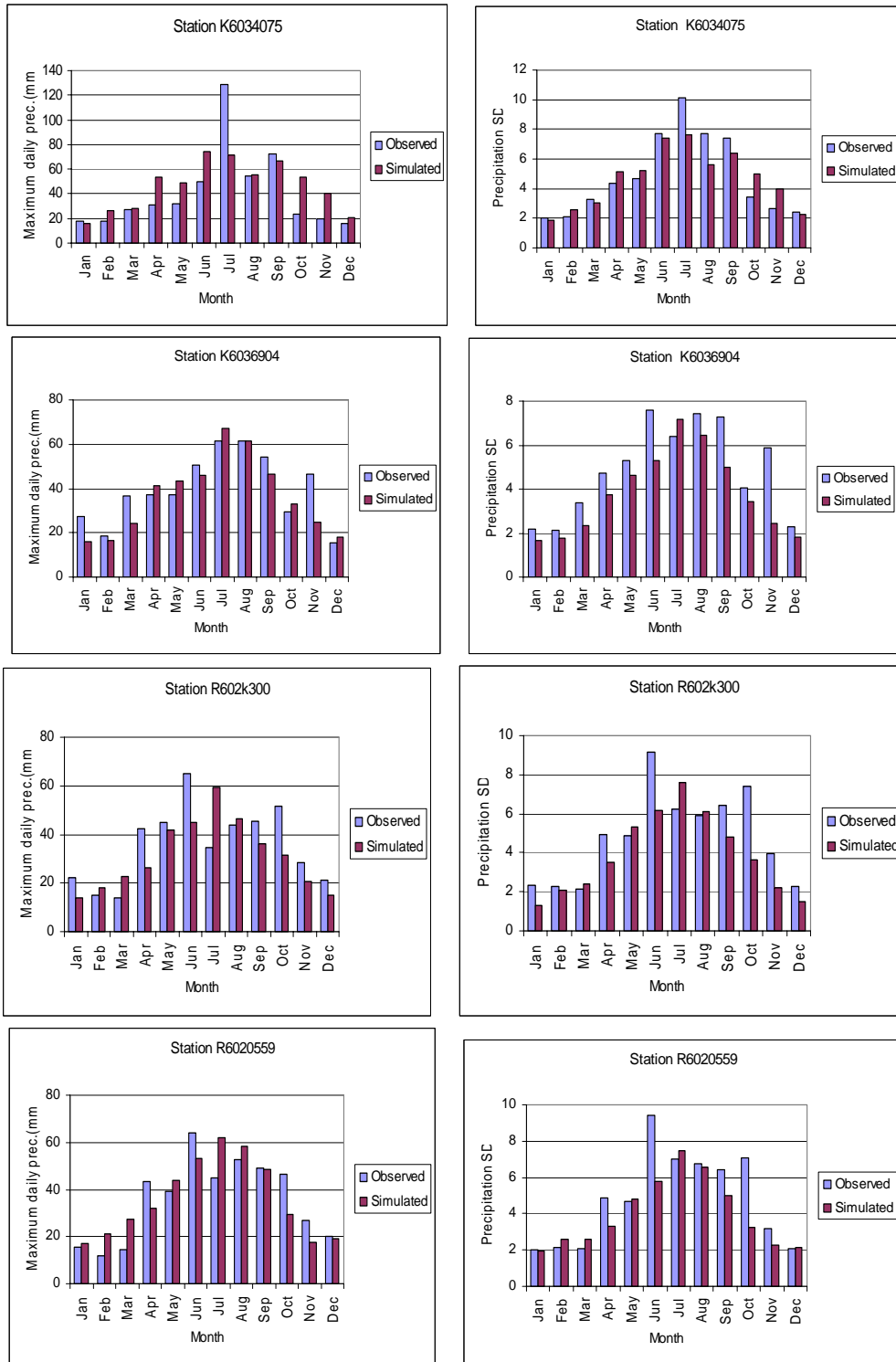


**Figure 10 - SDSM Validation Results of Downscaling Daily Precipitation in the Kenora and Rainy River Region**

**Table 10 - Downscaling Model Validation *RMSE* Statistics**

	Station Name	Station Number	Average Maximum Daily Precipitation (mm)	RMSE(mm)
Grand River Region	Brantford	G6140954	45.8	7.2
	Stratford	G6148105	46.6	15.0
	Glen Allan	G6142803	45.6	16.5
	Woodstock	G6149625	44.6	9.8
Kenora and Rainy River Region	Kenora A	K6034075	46.3	22.5
	Rawson Lake	K6036904	36.5	8.9
	Barwick	R6020559	35.8	10.1
	Emo Radbourne	R602K300	31.4	13.0

### **C. DOWNCALING CGCM2 OUTPUTS FOR THE FUTURE PERIOD**

Once the SDSM downscaling model has been calibrated and validated, the next step is to use the SDSM model to downscale the future climate change scenario simulated by the CGCM2. In this case, this means, the selected large-scale predictor variables to be used as input to each of the downscaling models are taken from CGCM2 simulation outputs. The data is divided into four distinct periods, namely, the current (covering the forty years period between 1961 and 2000), the 2020s (2010-2039), the 2050s (2040-2069) and the 2080s (2070-2099). The monthly statistics of the SDSM downscaling results for daily precipitation corresponding to the eight meteorological stations are summarized and plotted in Figure 11 and Figure 12. In general, the figures show consistent increasing trend in the predicted maximum precipitation. As compared to the current period (1961-2000), the maximum daily precipitation show an increasing trend for the 2050s and 2080s, while for the 2020s there is decreasing trend. This is consistent with the trends in the CGCM2 simulations.

Further screening of the predicted maximum precipitation (Figure 11 and Figure 12) indicates that the changes in the future precipitation are also season-dependent. However for heavy maximum daily precipitation occurring mostly between May and September, there is a consistent increasing trend for the 2050s and the 2080s. Such an increase in heavy daily rainfall will likely translate into significant increase in the corresponding design discharge.

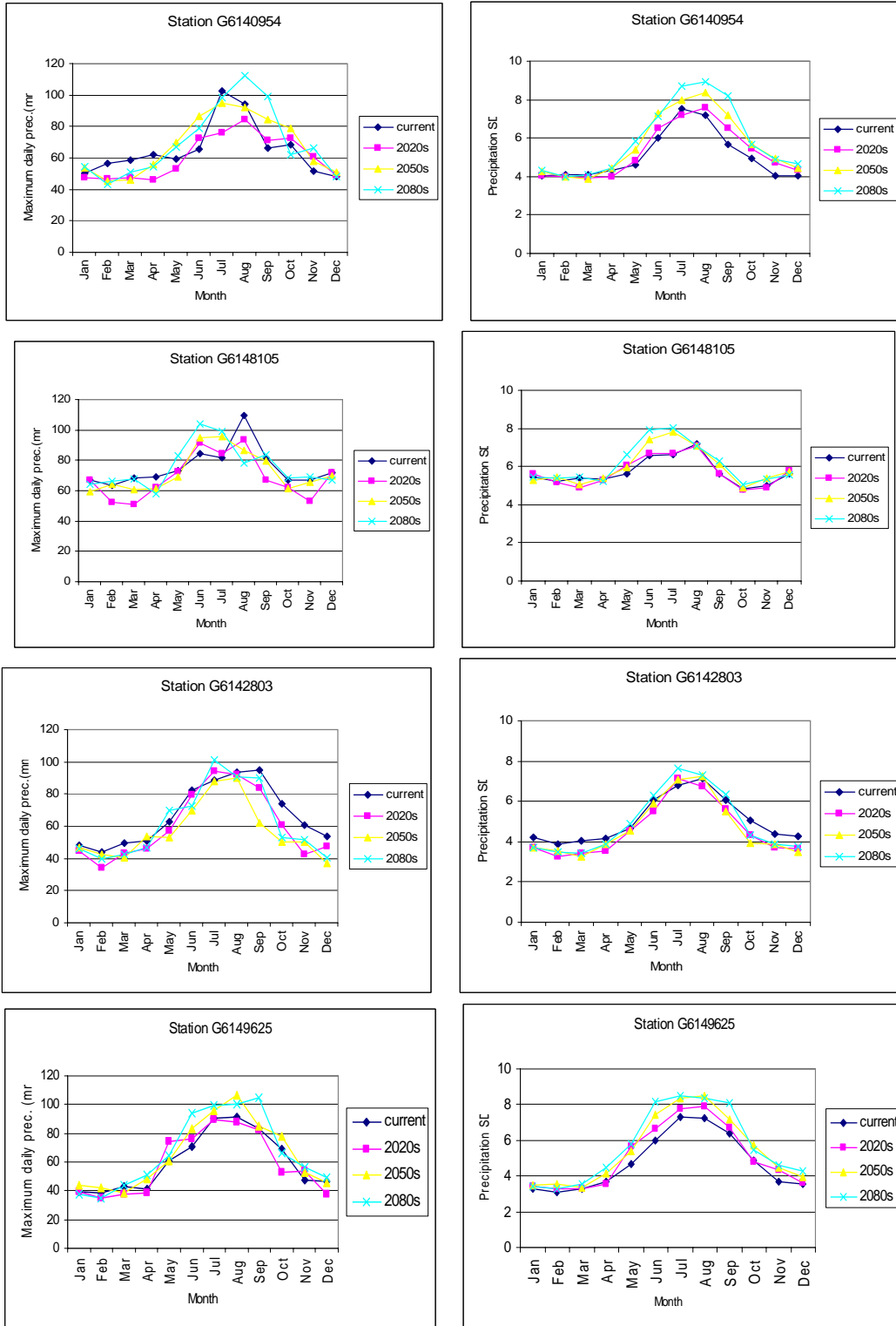


**Figure 11 - General Trend in Predicted Precipitation in the Grand River Region**

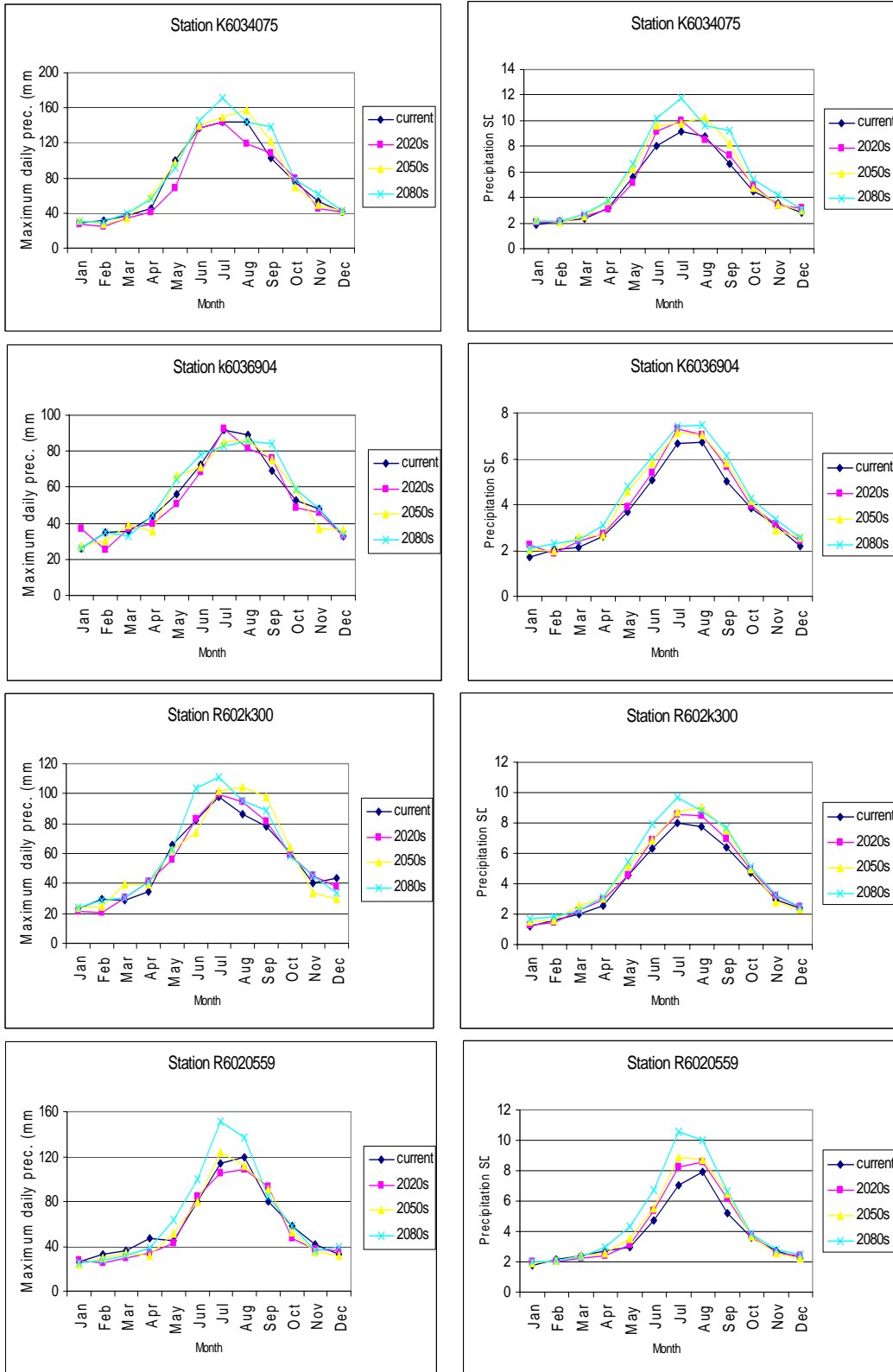


**Figure 12 - General Trend in Predicted Precipitation in the Kenora and Rainy River Region**

# Comparison of IDF Curves

---

As described earlier in chapter 4, we used the first 30 years (1961-1990) of the NCEP reanalysis data (as predictors) and the historical precipitation data (as predictand) for the downscaling model calibration at each station. The remaining ten years of data (1991-2000) are used for the validation of the downscaling model at each station. After we get the best statistical agreement between the observed and simulated maximum daily precipitation, the calibrated model is then used to downscale the precipitation data for the current (1961 to 2000) and future periods (namely, the 2020s the 2050s, and the 2080s) based on the CGCM2 predictors. Then we construct the IDF curves for the four periods: current, 2020s, 2050s and 2080s at each station.

We have also compared those IDF curves with those of the raw CGCM2 precipitation and with those of the observed precipitation for the current time period (1961-2000). The comparison results are presented here below. The main objective is to further assess whether the downscaling model provides more reliable future precipitation series as compared to the raw GCM simulations in this case. It is noteworthy that in some climate change impact studies, the raw GCM simulations are directly used.

## **A. COMPARISON OF IDF CURVES FOR THE CURRENT PERIOD**

### **1. THE GRAND RIVER REGION**

After constructing the IDF curves for the four stations in the Grand River Region, we compare the IDF curves of the raw CGCM2, the downscaled CGCM2 and the observed precipitation data for the current time period (1961-2000). Specifically, the raw CGCM2 precipitation is obtained from the CGCM2 outputs directly at the grid point 42.67°N, 78.75°W. To provide a clear comparison, we consider only the IDF curves corresponding to the 24-hour precipitation. The comparison is made for precipitation intensities starting from the 2-year up to the 100-year return periods.

Overall, the comparison results shown in Figure 13 and Figure 14 strongly confirm that the downscaled precipitation is consistently closer to the observed data than the raw CGCM2 simulations. This indicates that the downscaling model provides more reliable precipitation series as compared to the raw CGCM2 precipitation. Detailed analysis of those results is provided hereafter for each station.

#### **a. Station G6140954 (Brantford)**

Table-11 and Figure 13(A) show the difference between the precipitation corresponding to the raw CGCM2, the downscaled CGCM2 and the observed precipitation data. From

these results, it appears that while the raw CGCM2 data underestimated the precipitation intensity as compared with the observed data, the downscaled CGCM2 data are very close to the locally observed 24-hour precipitation.

**Table 11 - 24-hour Precipitation Comparison for the Current Period at Station G6140954**

Return period (yr)	2	5	10	20	50	100
Observed	51.6	65.2	74.2	82.9	94.1	102.5
Downscaled CGCM2	49.9	65.9	76.5	86.7	99.9	109.8
Raw CGCM2	51.9	62.0	68.7	75.1	83.4	89.6

**b. Station G6148105 (Stratford)**

Table 12 and Figure 13(B) show the difference between the predicted 24-hour precipitation for the raw CGCM2, the downscaled CGCM2 and the observed precipitation data. By comparing the corresponding IDF curves, it appears that the raw CGCM2 data significantly underestimated the precipitation compared to the observed data, while the downscaled CGCM2 data appear to provide more accurate local precipitation series as compared to the station data.

**Table 12 - 24-hour Precipitation Comparison for the Current Period at Station G6148105**

Return period (yr)	2	5	10	20	50	100
Observed	54.9	77.3	92.1	106.3	124.7	138.5
Downscaled CGCM2	56.7	79.4	94.3	108.7	127.3	141.2
Raw CGCM2	51.9	62.0	68.7	75.1	83.4	89.6

**c. Station G6142803 (Glen Allen)**

Once again, we consider the predicted 24-hour precipitation from the IDF curves corresponding to the 2-year up to 100-year return period. The results in Table-13 and Figure-13(C) confirm that the downscaled CGCM2 precipitation better represents the local information.

**Table 13 - 24-hour Precipitation Comparison for the Current Period at Station G6142803**

Return period (yr)	2	5	10	20	50	100
Observed	55.2	73.8	86.1	98.0	113.3	124.7
Downscaled CGCM2	50.4	71.8	86.0	99.6	117.2	130.4
Raw CGCM2	51.9	62.0	68.7	75.1	83.4	89.6

**d. Station G6146925 (Woodstock)**

Similar results are shown in Table 14 and Figure 13(D) for the station G6146925. Consistently, the results indicate that the downscaled CGCM2 data are the closest to the observed 24-hour precipitation.

**Table 14 - 24- hour Precipitation Comparison for the Current Period at Station G6149625**

Return period (yr)	2	5	10	20	50	100
Observed	58.9	78.7	91.8	104.3	120.6	132.8
Downscaled CGCM2	53.0	76.9	92.7	107.8	127.4	142.1
Raw CGCM2	51.9	62.0	68.7	75.1	83.4	89.6

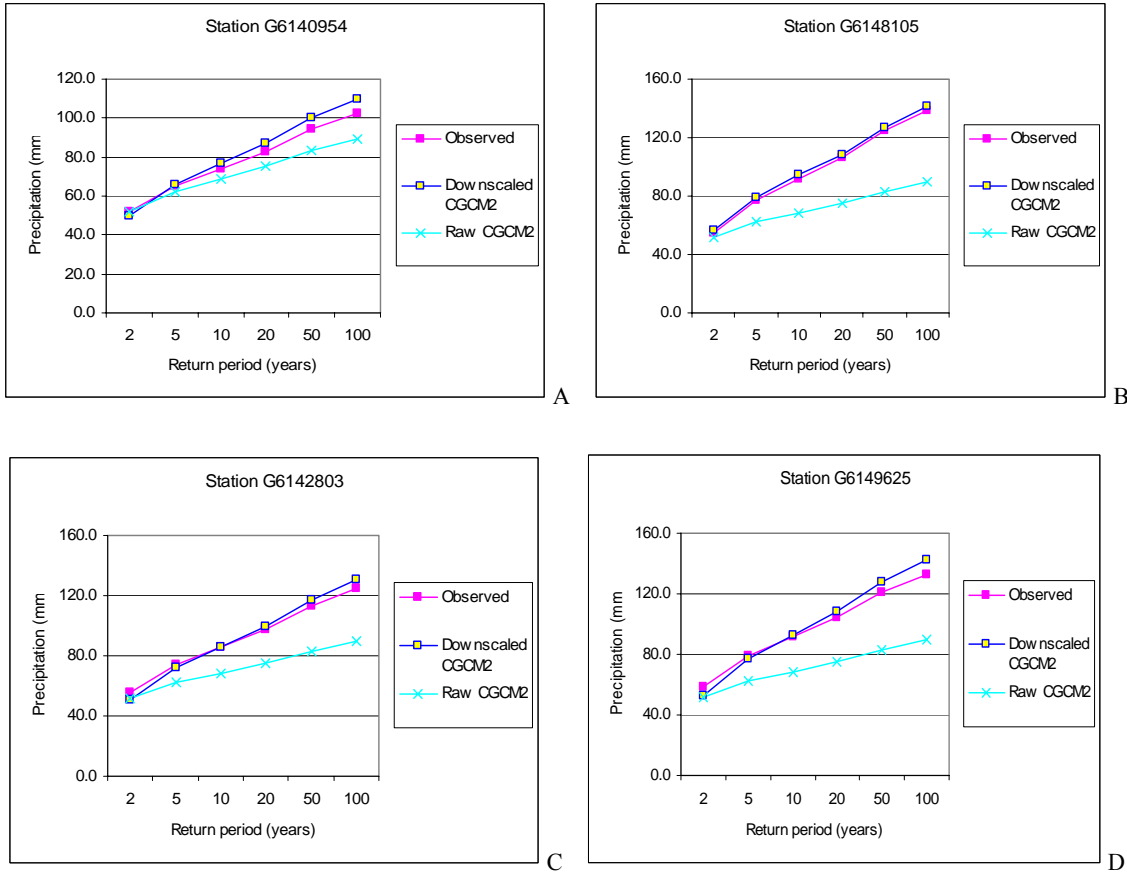


Figure 13 - 24-hr Precipitation Comparison for the Grand River Region

## **2. THE KENORA AND RAINY RIVER REGION**

After constructing the IDF curves for the four stations in the Kenora and Rainy River Region, we did the same comparison as presented previously for the Grand River Region. The raw CGCM2 precipitation, the downscaled CGCM2 and the observed precipitation data for the current time period (1961-2000) are compared. For the Kenora and Rainy River Region, the raw CGCM2 precipitation is obtained directly from the grid point 50.10°N, 93.75°W. Once again, to provide a clear comparison, only the IDF curves corresponding to the 24-hour precipitation are considered. The comparison is made for precipitation intensities starting from the 2-year up to the 100-year return periods.

The comparison results are summarized in Table 15 and Figure 14 for all the stations. It is shown (Table 15) that overall, the downscaled CGCM2 data are consistently close to the observed 24-hour precipitation whatever the station, while the raw CGCM2 data systematically underestimate the precipitation intensity compared with the observed data. This clearly explains the importance of downscaling in order to obtain accurate and reliable future precipitation series for the specific area where climate change impact is to be investigated.

Furthermore, the above comparison results indicate that the downscaling model can be used to generate the future climate scenarios for the selected study areas.

**Table 15 - 24-Hour Precipitation Comparison for the Current Period in the Kenora and Rainy River Region**

Station Number	Return period (yr)	2	5	10	20	50	100
K6034075	Observed	60.4	89.7	109.1	127.7	151.8	169.8
	Downscaled CGCM2	59.7	87.5	105.8	123.4	146.2	163.3
	Raw CGCM2	45.8	61.6	72.1	82.2	95.3	105.1
K6036904	Observed	57.7	77.6	90.7	103.4	119.7	132.0
	Downscaled CGCM2	49.1	74.5	91.2	107.3	128.1	143.8
	Raw CGCM2	45.8	61.6	72.1	82.2	95.3	105.1
R6020559	Observed	57.8	85.3	103.6	121.1	143.7	160.7
	Downscaled CGCM2	52.4	81.9	101.4	120.1	144.4	162.5
	Raw CGCM2	45.8	61.6	72.1	82.2	95.3	105.1
R602K300	Observed	56.6	78.2	92.5	106.2	124.0	137.3
	Downscaled CGCM2	56.9	81.8	98.2	114.0	134.5	149.8
	Raw CGCM2	45.8	61.6	72.1	82.2	95.3	105.1

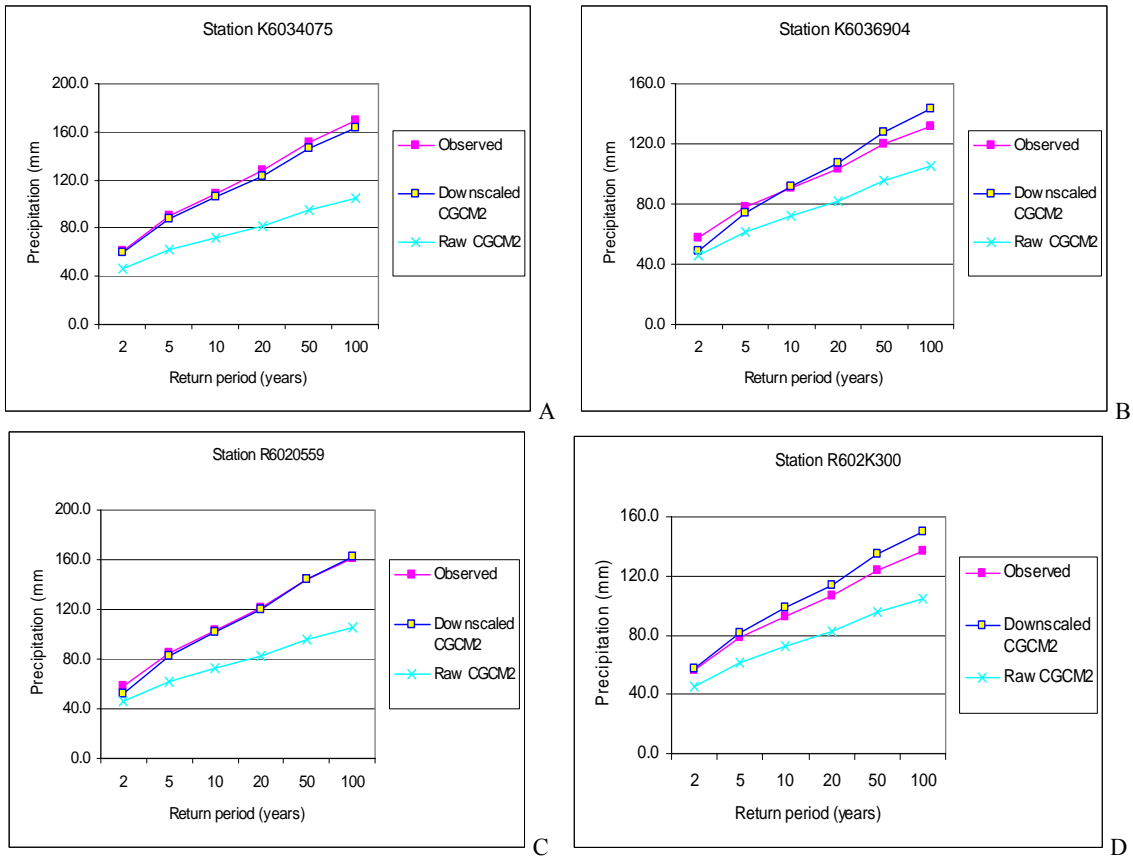


**Figure 14 - 24-hour Precipitation Comparison in the Kenora and Rainy River Region**

## **B. COMPARISON OF IDF CURVES FOR THE FUTURE PERIOD**

### **1. THE GRAND RIVER REGION**

After the above analysis, we used the calibrated downscaling model to generate the precipitation data for the current (1961 to 2000) and future periods (2020s, 2050s, 2080s) based on the CGCM2 predictors. Then we constructed the IDF curves for the four periods at each station. The main objective is to estimate the changes in the predicted precipitation intensity as compared with the current period precipitation intensity. Different rainfall durations (ranging from 0.5-hour to 24-hour) and return periods (ranging from 2-year to 100-year) are considered. The analysis results are presented and discussed for each station in the following.

#### **a. Station G6140954 (Brantford)**

The IDF curves for the four selected time periods: current, 2020s, 2050s and 2080s at station G6140954 are constructed respectively. Figure 15 shows the IDF curves for different rainfall durations at station G6140954. It appears that the precipitation intensity with the same duration and return period has consistently increased from the current to the 2050s and thereafter with a significant increase in 2080s except 2020s with a slight decrease. To further assess the changes in the rainfall intensity, Table A9 (in Appendix) summarizes the current and predicted rainfall intensities along with the percentage of increase for different rainfall durations and return periods. Precisely, for the 2-year and 5-year return period, whatever the rainfall duration, the rainfall intensity has increased by about 10% to 37% for the 2050s and the 2080s. For the 10-year and 20-year return period, the increase in the rainfall intensity ranges from 24% to 49% for the 2050s and 2080s, while for the 50-year and 100-year return period, the increase in rainfall intensity is about 31% to 57%.

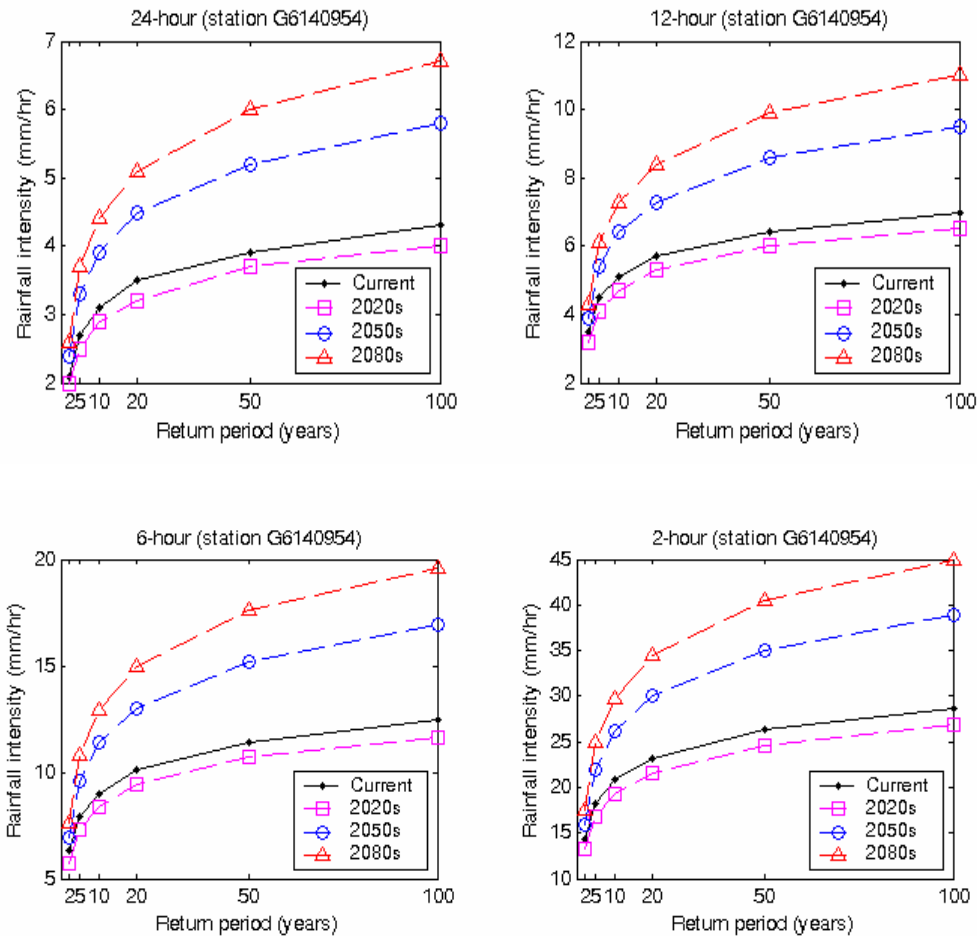


**Figure 15 – Historical and Predicted Rainfall Intensity at Station G6140954**

**b. Station G6148105 (Stratford)**

Figure 16 shows the IDF curves for different rainfall durations at station G6148105. It appears that the precipitation intensity with the same duration and return period has consistently increased from the current to the 2050s and thereafter with a significant increase in 2080s except 2020s with a decrease. To further assess the changes in the rainfall intensity, Table A10 (in Appendix) summarizes the current and predicted rainfall intensities along with the percentage of increase for different rainfall durations and return periods. Precisely, for the 2-year and 5-year return period, whatever the rainfall duration, the rainfall intensity has increased by about 5 % to 16% for the 2050s and the 2080s. For the 10-year and 20-year return period, the increase in the rainfall intensity ranges from 13% to 23% for the 2050s and 2080s, while for the 50-year and 100-year return period, the increase in rainfall intensity is about 14% to 25% respectively.

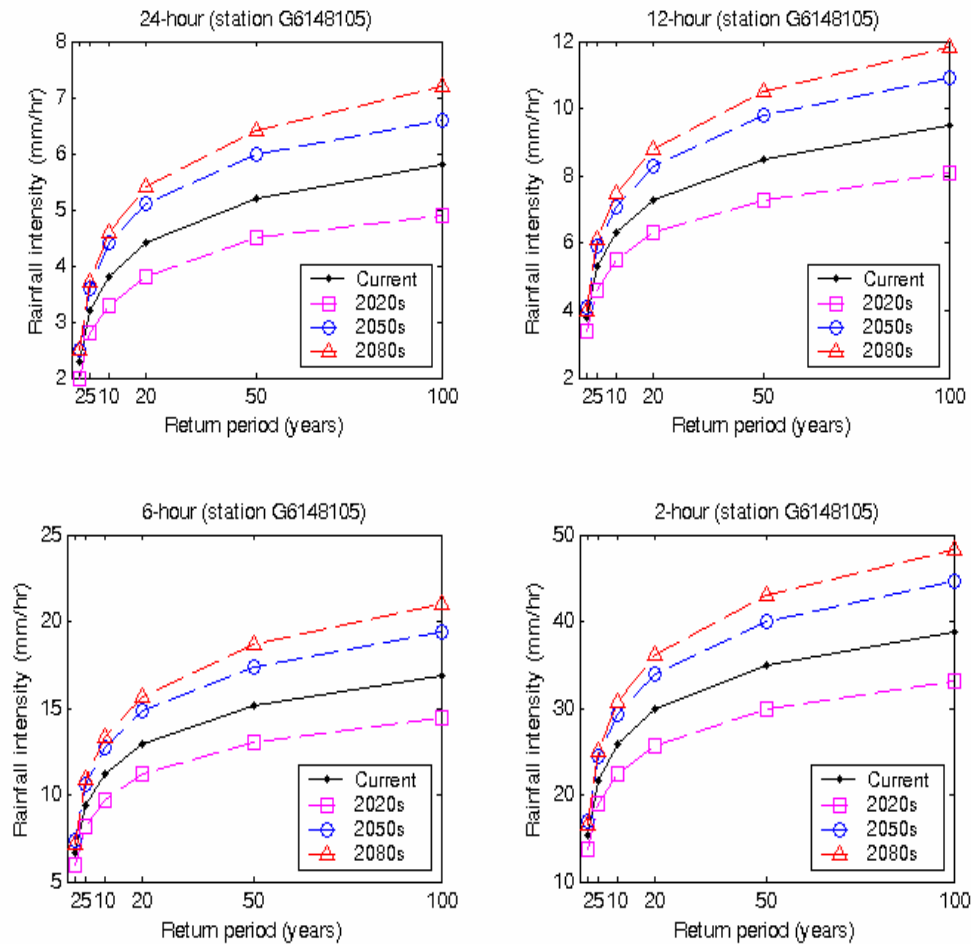


**Figure 16 - Historical and Predicted Rainfall Intensity at Station G6148105**

**c. Station G6142803 (Glen Allen)**

Figure 17 shows the IDF curves for different rainfall durations at station G6142803. It appears that the precipitation intensity with the same duration and return period has consistently decreased from the current to the 2050s and 2080s, thereafter with a significant decrease in 2020s. To further assess the changes in the rainfall intensity, Table A11 (in Appendix) summarizes the current and predicted rainfall intensities along with the percentage of change for different rainfall durations and return periods. Precisely, for the 2-year and 5-year return period, whatever the rainfall duration, the rainfall intensity has decreased by about 4 % to 11 % for the 2050s and 2080s. For the 10-year and 20-year return period, the decrease in the rainfall intensity ranges from 7 % to 12 % for the 2050s

and 2080s, while for the 50-year and 100-year return period, the decrease in rainfall intensity is about 5 % to 13 %. These results are consistent with the trend analysis results discussed earlier.

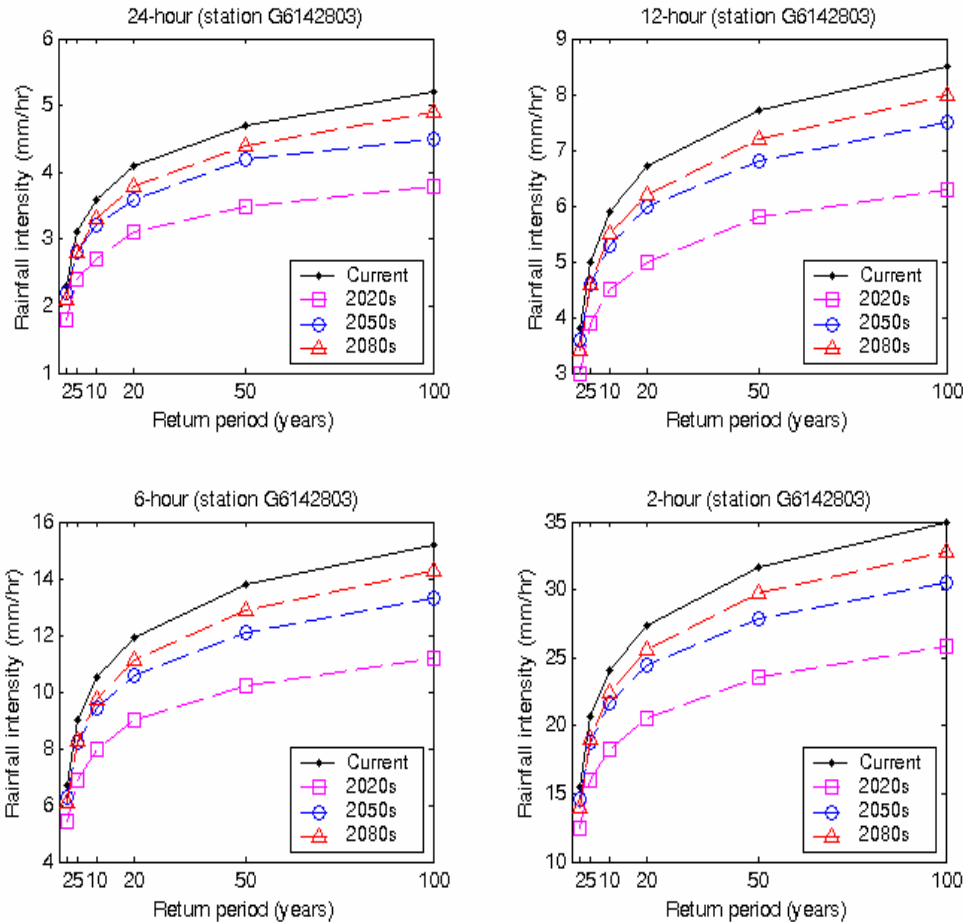


**Figure 17 - Historical and Predicted Rainfall Intensity at Station G6142803**

**d. Station G6149625 (Woodstock)**

Figure 18 shows the IDF curves for different rainfall durations at station G6149625. It appears that the precipitation intensity with the same duration and return period has consistently increased from the current to the 2050s and thereafter with a significant increase in 2080s except 2020s with a decrease. To further assess the changes in the rainfall intensity, Table A12 summarizes the current and predicted rainfall intensities along with the percentage of increase for different rainfall durations and return periods. Precisely, for the 10-year and 20-year return period, the increase in the rainfall intensity

ranges from 13 % to 32 % for the 2050s and 2080s, while for the 50-year and 100-year return period, the increase in rainfall intensity is about 21% to 40%.

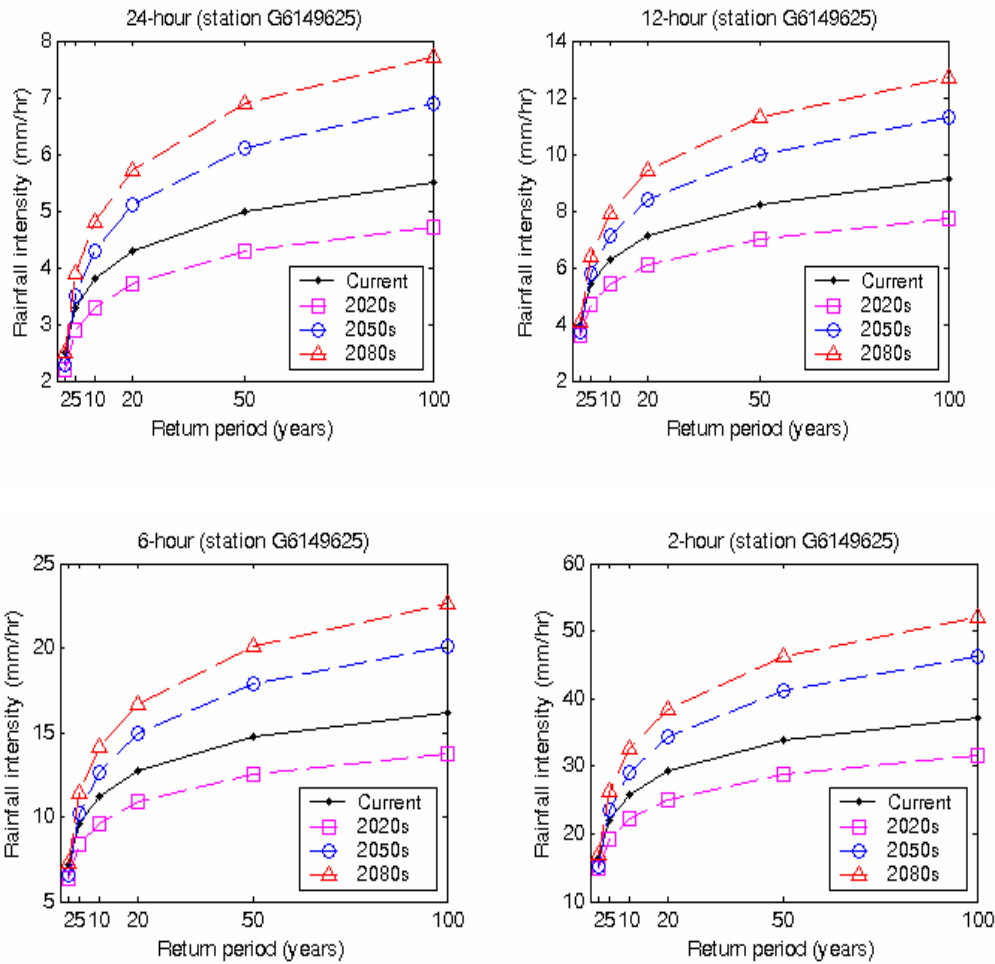


**Figure 18 - Historical and Predicted Rainfall Intensity at Station G6149625**

## **2. THE KENORA AND RAINY RIVER REGION**

Similar to the Grand River Region, we used the calibrated downscaling model to downscale the precipitation data for the current and future periods based on the CGCM2 predictors. Then we constructed the IDF curves for the four periods (current, 2020s, 2050s, 2080s) at each station. Detailed results are reported hereafter for each station in the Kenora and Rainy River Region.

### **a. Station K6034075 (Kenora A)**

The IDF curves for the four selected time periods: current, 2020s, 2050s and 2080s at station K6034075 are constructed respectively. Figure 19 shows the IDF curves for different rainfall durations at station K6034075. It appears that the precipitation intensity with the same duration and return period has consistently increased from the current to the 2050s and thereafter with a significant increase in 2080s except 2020s with a significant decrease. To further assess the changes in the rainfall intensity, Table A13 summarizes the current and predicted rainfall intensities along with the percentage of increase for different rainfall durations and return periods. Precisely, for the 2-year and 5-year return period, whatever the rainfall duration, the rainfall intensity has increased by about 10% to 36% for the 2050s and the 2080s. For the 10-year and 20-year return period, the increase in the rainfall intensity ranges from 19 % to 39 % for the 2050s and 2080s, while for the 50-year and 100-year return period, the increase in rainfall intensity is about 23 % to 41 %.

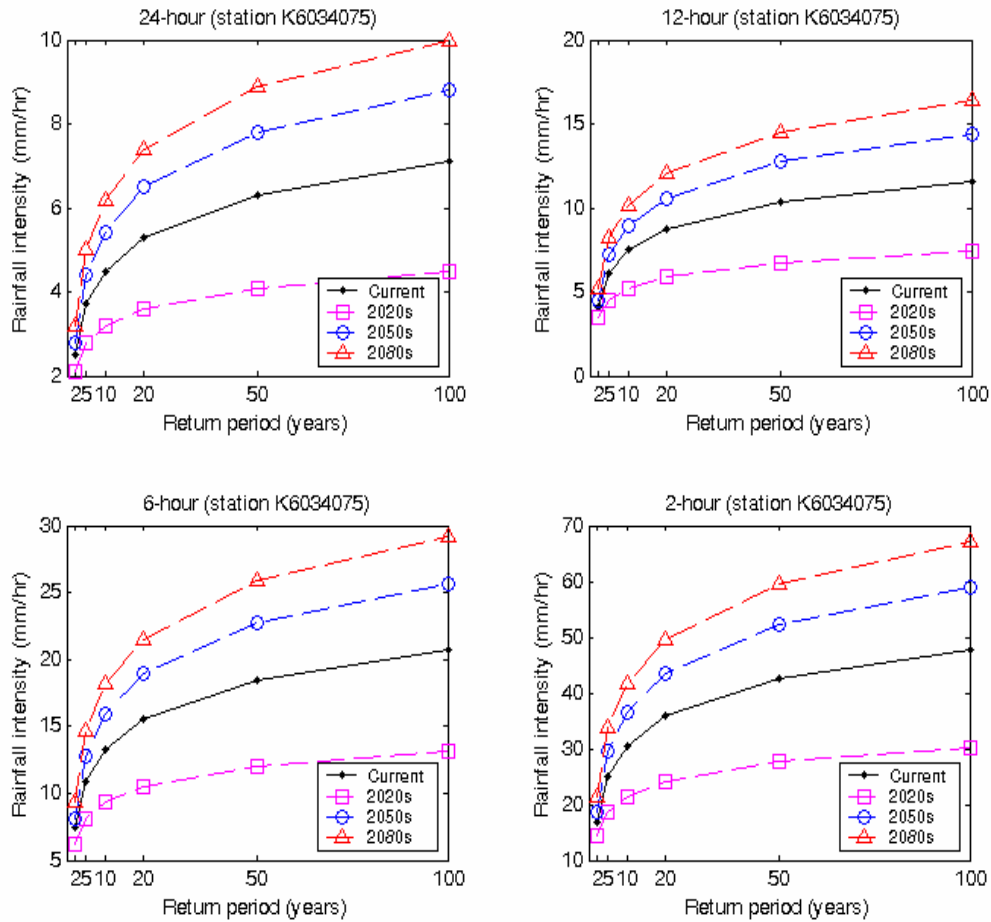


**Figure 19 - Historical and Predicted Rainfall Intensity at Station K6034075**

**b. Station K6036904 (Rawson Lake)**

Figure 20 shows the IDF curves for different rainfall durations at station K6036904. It appears that the precipitation intensity with the same duration and return period has consistently increased from the current to the 2050s and thereafter with a significant increase in 2080s except 2020s with a decrease. To further assess the changes in the rainfall intensity, Table A14 summarizes the current and predicted rainfall intensities along with the percentage of increase for different rainfall durations and return periods. Precisely, for the 10-year and 20-year return period, the increase in the rainfall intensity ranges from 11 % to 23 % for the 2050s and 2080s, while for the 50-year and 100-year return period, the increase in rainfall intensity is about 18 % to 30 %.

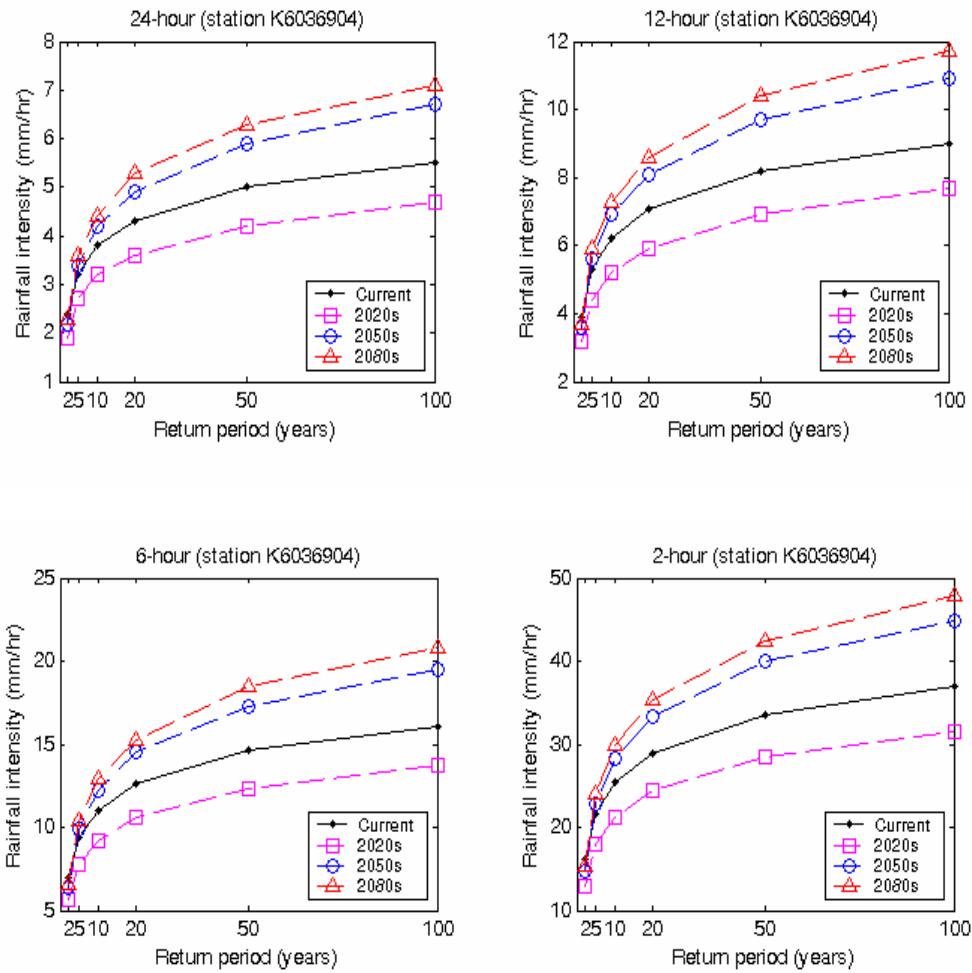


**Figure 20 - Historical and Predicted Rainfall Intensity at Station K6036904**

**c. Station R6020559 (Barwick)**

The IDF curves for the four selected time periods: current, 2020s, 2050s and 2080s at station R6020559 are constructed respectively. Figure-21 shows the IDF curves for different rainfall durations at station R6020559. It appears that the precipitation intensity with the same duration and return period has consistently increased from the current to the 2050s and thereafter with a significant increase in 2080s except 2020s with a decrease. To further assess the changes in the rainfall intensity, Table – A15 summarizes the current and predicted rainfall intensities along with the percentage of increase for different rainfall durations and return periods. Precisely, for the 10-year and 20-year return period, the increase in the rainfall intensity ranges from 15 % to 28 % for the 2050s and 2080s, while for the 50-year and 100-year return period, the increase in rainfall intensity is about 20 % to 30 %.

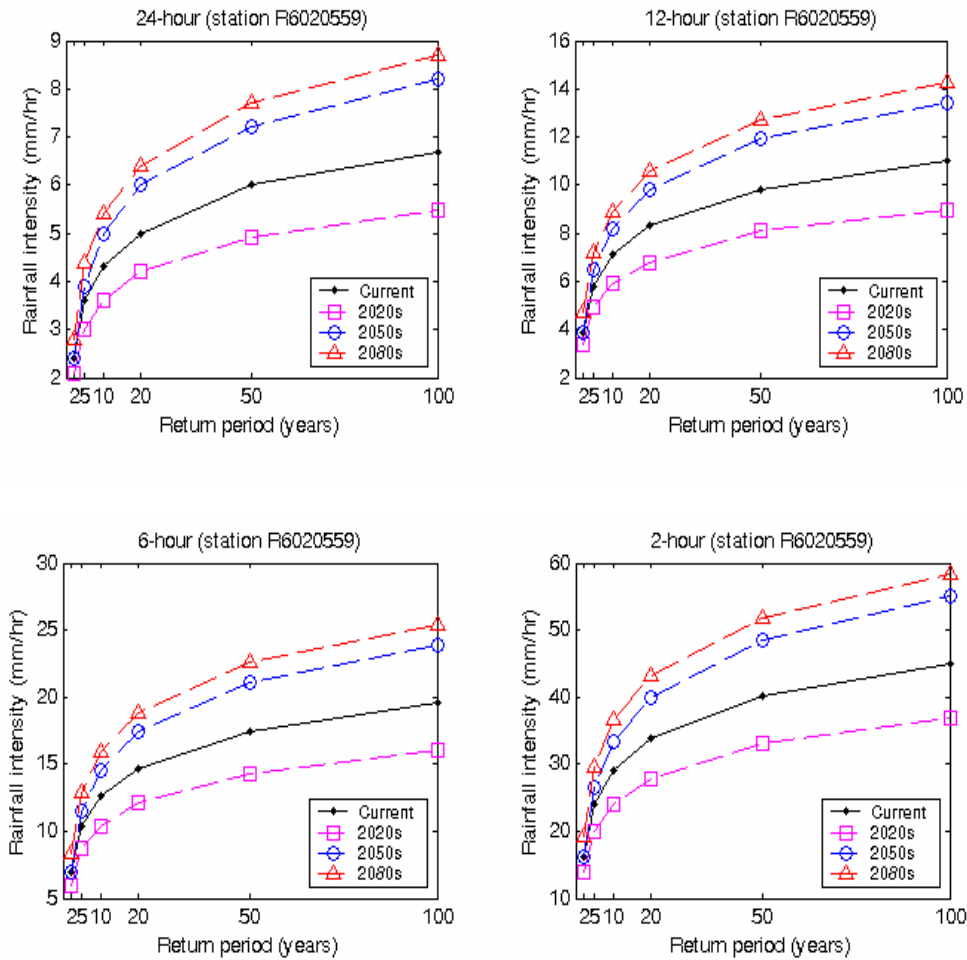


**Figure 21 - Historical and Predicted Rainfall Intensity at Station R6020559**

**d. Station R602K300 (Emo Radbourne)**

Figure 22 shows the IDF curves for different rainfall durations at station R602K300. It appears that the precipitation intensity with the same duration and return period has consistently increased from the current to the 2050s and thereafter with a significant increase in 2080s except 2020s with a slight decrease. To further assess the changes in the rainfall intensity, Table A16 summarizes the current and predicted rainfall intensities along with the percentage of increase for different rainfall durations and return periods. Precisely, for the 2-year and 5-year return period, whatever the rainfall duration, the rainfall intensity has increased by about 8 % to 21 % for the 2050s and the 2080s. For the 10-year and 20-year return period, the increase in the rainfall intensity ranges from 13 % to 25 % for the 2050s and 2080s, while for the 50-year and 100-year return period, the increase in rainfall intensity is about 13 % to 25 %.

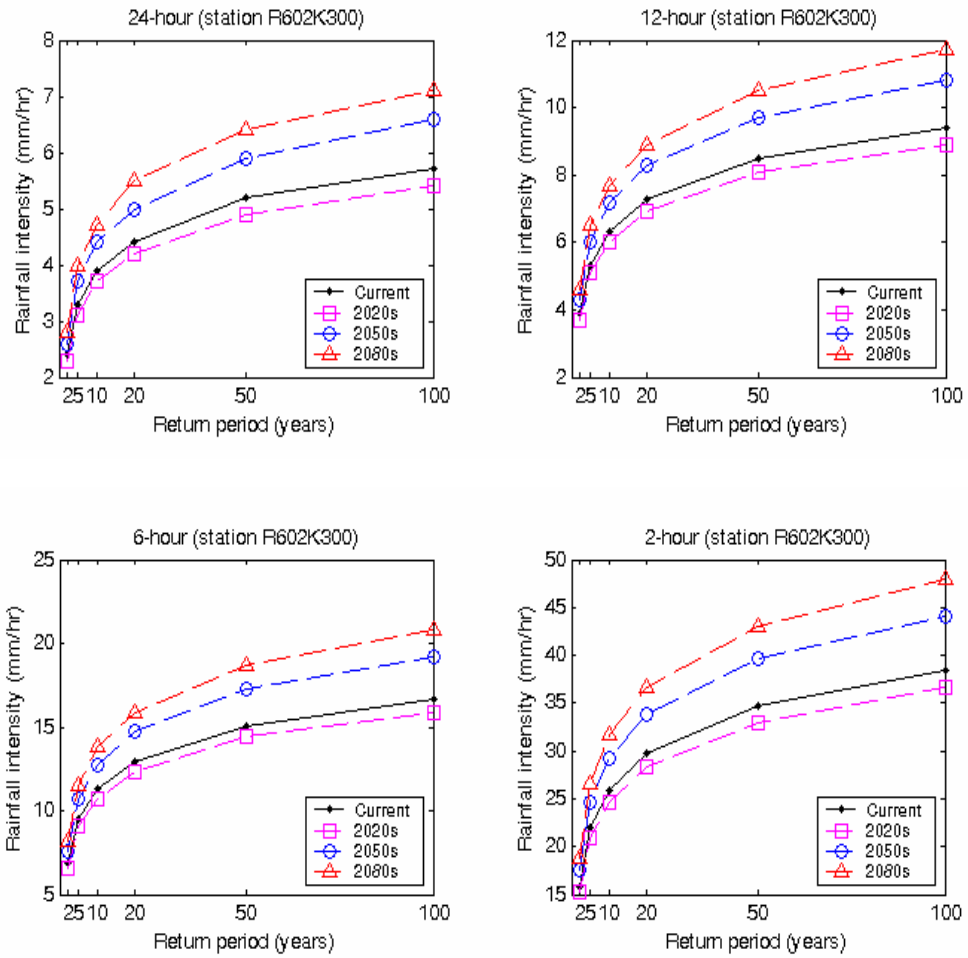


**Figure 22 - Historical and Predicted Rainfall Intensity at Station R602K300**

## **C. SUMMARY OF THE IDF CURVES COMPARISON**

Based on the first part of the above analysis and comparison of the IDF curves for each station, the raw CGCM2 has always underestimated the precipitation intensity as compared to the observed data, while the downscaled data are found consistently close to the observed local precipitation whatever the station. This justifies the need of downscaling to generate local precipitation data for the current and future periods.

From the second part of the analysis dealing with the IDF curves for the current and the future periods, striking changes in the precipitation intensity between the current and the future time periods are shown. Overall, there is a significant increase in the rainfall intensity for the 2050s and the 2080s whatever the duration and the return considered. At all the stations except station G6142803, similar increasing trends are shown from the current to the 2080s time period. The trends are always increasing from current to the future, except for 2020s where there is a decrease which may be related to the CGCM2 simulations

From the summary Tables (Table A9 to Table A16) in the Appendix, it is also shown that overall, rainfall intensities with X-year return period ( $X= 5, 10, 20, 50, 100$ ) under current climate conditions are almost equal to those with  $(X/2)$ -year return period under future climate conditions. As an example, rainfall intensities with 10-year return period under current climate conditions are almost equal to those with 5-year return period under predicted climate conditions. Given that in Ontario, most of the storm drainage systems are design for 10-year whereas bridges and culverts are designed for 20 or 50-year depending upon total span of the structure, it appears that most of the highway infrastructures can be significantly affected by the heavy rainfall intensity predicted in the study area. As an example, an actual 10-year drainage system will be able to withstand only 5-year storms by 2050s, whereas a current 50-year drainage structure will be able to handle only 20-year storms by 2050s. Therefore possible impact of anticipated climate change on drainage structures can range from capacity shortage to total destruction. To further assess this potential impact, a design experiment is considered in the following.

# Rational Method Design for Highway Drainage Infrastructure

---

## A. DESIGN PROCEDURE

To further assess the potential impact of climate change on drainage infrastructure, a design experiment for a storm sewer pipe is applied in the Grand River Region and the Kenora and Rainy River Region respectively. In this design experiment, we used the rational method (Chow et al, 1988) whereby peak flow ( $Q$ ) is given by:

$$Q=0.278CIA \quad (\text{Eq. 8})$$

where

$Q$  = peak flow ( $\text{m}^3/\text{s}$ )

$C$  = runoff coefficient ( $0 \leq C \leq 1$ )

$I$  = average precipitation intensity over a given duration for return period  $T$  ( $\text{mm}/\text{h}$ )

$A$  = basin area ( $\text{km}^2$ )

Here, the drainage basin area is determined using a topographic map. The topographic map provided the areas and slopes of each drainage basin. The time of concentration ( $T_c$ ) of the drainage basin is estimated using Kirpich empirical equation. This time is necessary to determine the intensity ( $I$ ) from the IDF curves. The runoff coefficient is determined based on various factors such as soil groups, land slope, and land use. With the estimated design discharge  $Q$ , Manning's equation was used to determine the pipe diameter as follows

$$Q = \frac{1.486}{n} AR_h^{2/3} S_0^{1/2} \quad (\text{Eq. 9})$$

where

$n$  = Manning's roughness coefficient

$A$  = pipe cross-sectional area ( $\text{m}^2$ )

$R_h$  = wetted perimeter of pipe (m)

$S_o$  = pipe slope (m/m).

In storm drainage design by the rational method, pipes are sized to convey the peak discharge estimated by the rational method, when flowing full. For full-flow pipe  $R_h = D/4$  ( $D$  = pipe diameter). So we can determine the pipe diameter ( $D$ ) as follows

$$D = \left( \frac{3.21Qn}{\sqrt{S_o}} \right)^{3/8} \quad (\text{Eq. 10})$$

In this design experiment, the precipitation intensities corresponding to the future time periods are calculated by applying the changes in rainfall intensities between the current and future time periods on the observed intensities of the historical data. Given that the precipitation intensity is shown to decrease for the 2020s at all the stations considered, thus there is no concern regarding the operational capacity of the drainage infrastructures. Therefore, in the design experiment, we consider only the 2050s and 2080s periods where increasing rainfall intensity is predicted.

## **B. CASE STUDY**

Specifically, two design cases are considered. The first one in the Grand River Region, and the second one in the Kenora and Rainy River Region. The detailed calculations to determine the pipe diameter in the selected areas were made on a spreadsheet, and are presented in Table A17 and Table A18 in the Appendix.

### **1. GRAND RIVER REGION**

In this case, only the meteorological station G6140954 (Brantford) is used. By applying the rational method and the Manning equation, the changes in the estimated pipe diameter as compared with the current pipe diameter, are shown in Figure 23. Table 16 summarizes the changes (in percentage) in the pipe diameter by 2050s and 2080s as compared to current design standards. It appears that for the commonly used 10-year drainage system, the pipe diameter should be increased by about 10% and 16% by 2050s and 2080s respectively in order to maintain the present level of operational capability.

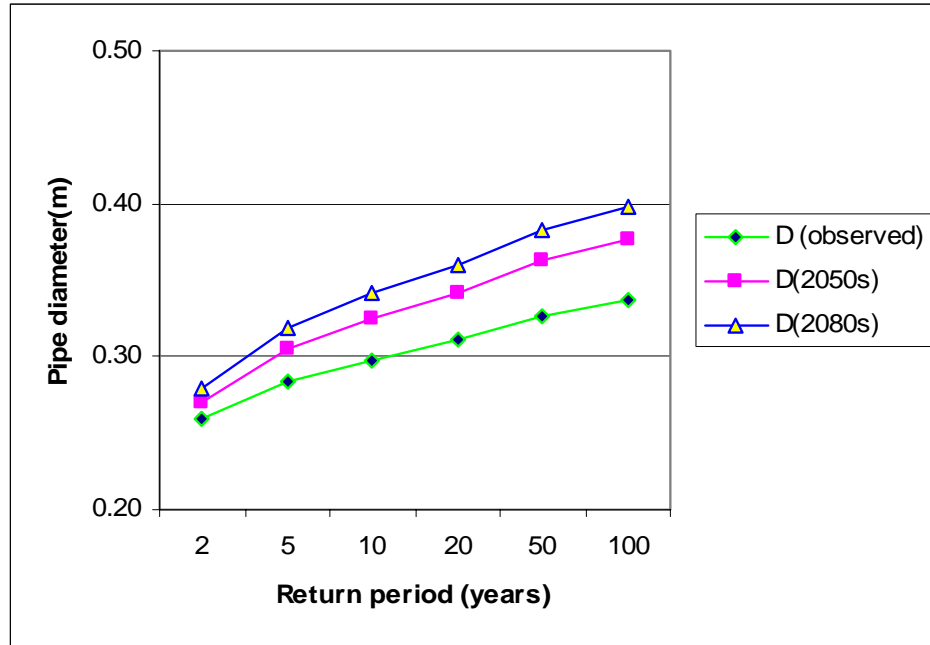


**Figure 23 – Estimated Pipe Diameter for 2050s and 2080s Compared with the Current Period in the Grand River Region**

## 2. KENORA RAINY RIVER REGION

In this case, only the meteorological station K6034075 (Kenora A) is used. By applying the rational method and the Manning equation, the changes in the estimated pipe diameter as compared with the current pipe diameter are shown in Table 16 for the different return periods. Figure 24 highlights the change in the corresponding pipe diameter necessary to safely drain the predicted peak flow. For a 10-year drainage structure, the pipe diameter should be increased by about 7 % and 12.5 % by 2050s and 2080s respectively in the Kenora and Rainy River Region.

In general, in order to account for climate change impact on drainage infrastructure in southern and northern Ontario, an average increase of about 16% in pipe diameters is needed for all sewer pipes. For larger structures (e.g. bridges and culverts), an update of the design standards is needed given the predicted significant increase (about 31% to 57% in average) in the rainfall intensity for the 50 and 100-year storms.

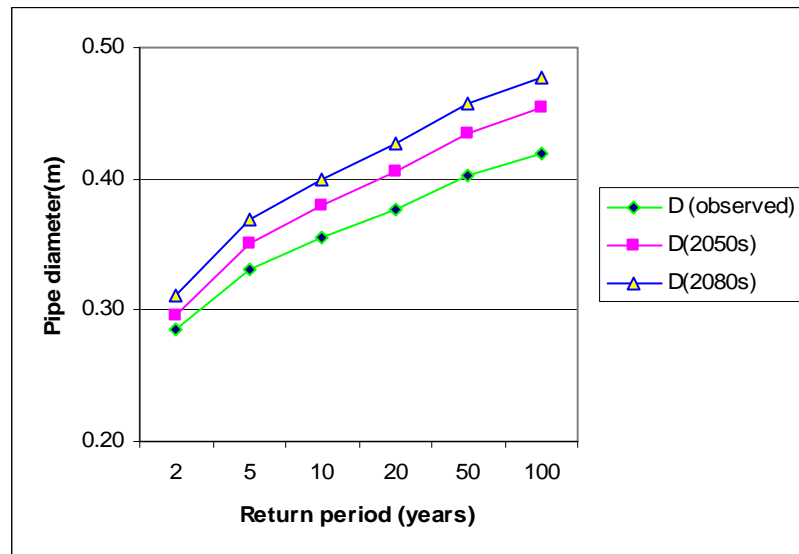


**Figure 24 – Estimated Pipe Diameter for 2050s and 2080s Compared with the Current Period in the Kenora and Rainy River Region**

**Table 16 - Change in Pipe Diameter for 2050s and 2080s Compared with the Current Period in Ontario**

Return period (yr)			2	5	10	20	50	100
Change in pipe diameter (%)	Grand River Region	2050s	3.6	7.3	8.9	10.1	11.4	12.1
		2080s	7.5	12.3	14.4	15.9	17.5	18.4
	Kenora and Rainy River Region	2050s	3.6	6.1	7.0	7.5	8.1	8.4
		2080s	9.4	11.7	12.5	13.0	13.5	13.8

# Summary and Conclusions

---

This final report provides a comprehensive analysis results on climate change impact on the future highway drainage infrastructures in Ontario. First of all, the emphasis in this report was given to identify the trends of the observed precipitation data. By using the Mann-Kendall trend test, increasing trends in the precipitation data of the Grand River Region and the Kenora and Rainy River Region are shown. For the annual maximum daily precipitation, there are increased trends for three of the four stations (G6140954, G6148105 and G6149625) in the Grand River Region and for all the four stations (K6034075, K6036904, R6020559 and R602k300) in the Kenora and Rainy River Region.

In addition, in order to assess whether there is a change in the frequency and intensity of the maximum precipitation events in the recent decades, the historical daily data at each recording station in the Grand River Region is divided into two periods. Then, IDF curves are constructed for each period. By comparing the IDF curves for the two periods, it is shown that the intensity of the observed 24-hour precipitation has significantly increased in the last two decades (1980s -2000).

CGCM2 outputs are successfully downscaled into more accurate local scale daily precipitation series using the SDSM model. Analysis and comparison of IDF curves based on the downscaled data (current and future climate conditions) revealed striking changes in the precipitation intensity between the current and the future time periods (2050s and 2080s) whatever the duration and return period considered. At almost all the stations, similar increasing trends are shown from the current to the 2080s time period. The trends are always increasing from current to the future, except for 2020s where there is a decrease which may be related to the CGCM2 simulations.

Specifically, it is shown that an actual 10-year drainage system will be able to withstand only 5-year storms by 2050s, whereas a current 50-year drainage structure will be able to handle only 20-year storms by 2050s. Given that in Ontario, most of the storm drainage systems are design for 10-year whereas bridges and culverts are designed for 20 or 50-year depending upon total span of the structure, it appears that most of the highway infrastructures can be significantly affected by the heavy rainfall intensity predicted in southern and northern Ontario.

Finally, we estimated the effect of the anticipated changes in the intensity and frequency of the future storm events on the existing drainage facilities. Two design experiments are considered. The results indicate a significant change in the design discharge and the corresponding pipe diameter necessary to safely drain the peak flow. It is shown that for the commonly used 10-year drainage system, the pipe diameter should be increased by

about 10% and 16% by 2050s and 2080s respectively in order to maintain the present level of operational capability in southern Ontario. Slightly similar results are found in northern Ontario. Therefore, it is suggested that an increase of about 16% in pipe diameter would be necessary for all sewer pipes in order to maintain the present level of operational capability of highway drainage infrastructures in Ontario.

# Recommendations

---

Overall, the study results indicate strong and significant increase (about 24% and 35% in average) in the rainfall intensity by 2050s and 2080s respectively. It is found that rainfall intensities with X-year return period under current climate conditions are almost equal to those with (X/2)-year return period under predicted climate conditions. As an example, it is shown that actual 10-year drainage structure will be able to withstand only 5-year storms by 2050s, whereas a current 50-year drainage structure will be able to handle only 20-year storms by 2050s. In general, the study results suggest that a change in drainage design standards is needed to safely sustain future heavy storm events. Therefore, there is a need of recommendations for revising the existing design standards to account for the changing climate conditions and avoid an increase in the risk of “failure” of the highway drainage infrastructures.

## **Recommendations for future work**

The preliminary study results indicate increasing trend in both historical and future maximum daily precipitation in most of the selected study areas. Further study should include other regions across Ontario and a larger number of stations.

Given that the preliminary study uses one GCM and one climate change scenario along with one downscaling method, there is a need of further study, including other GCMs and RCMs, different climate change scenarios, and downscaling techniques.

A thorough investigation of uncertainty due to the downscaling methods and the GCM and/or RCM predictions is also required before making-decision on possible adaptation of design standards. Ensemble analysis approach should be considered to capture all range of uncertainties.

# Acknowledgements

---

This work was made possible through a research grant from the Highway Infrastructure Innovation Funding Program, Ministry of Transportation of Ontario. The authors acknowledge the assistance of the staff of the Ministry of Transportation of Ontario, in particular, the contribution of Dr. Hani Farghaly in the selection of the study areas. The authors gratefully acknowledge the contribution of Dr. Yonas Dibike at the earlier stage of the study.

# References

---

Burn, D.H., and Hag-Elnur, M.A., "Detection of hydrologic trend and variability", *Journal of Hydrology*, Vol. 255, 2002, pp. 107-122.

Chow, Ven T., Maidment, David R., and Mays, Larry W., *Applied Hydrology*, McGraw Hill, Inc., Columbus, 1988, pp. 467-470.

Coulibaly, P., and Dibike, Y.B., "Downscaling of Global Climate Model Outputs for Flood Frequency Analysis in the Saguenay River System", Final Report submitted to Climate Change Action Fund, Environment Canada, 2004, p. 84.

Denault, C., R.G. Millar, and B.J. Lence, "Climate Change and Drainage Infrastructure Capacity in an Urban Catchment", *Proceedings of CSCE 30th Annual Conference*, Montreal, 2002.

Douglas, E.M., Vogel, R.M., and Kroll, C.N., "Trends in Floods and Low Flows in the United States: Impact of Spatial Correlation", *Journal of Hydrology*, Vol. 240, 2000, pp. 90-105.

Dibike, Y. B., and Coulibaly, P., "Hydrologic Impact of Climate Change in the Saguenay Watershed: Comparison of Downscaling Methods and Hydrologic Models", *Journal of Hydrology*, Vol. 307, 2005, pp.145-163.

Gan, T.Y., "Finding Trends in Air Temperature and Precipitation for Canada and North-eastern United States", In: Kite, G.W. and Harvey, K.D., Editors, 1992. *Using Hydrometric Data to Detect and Monitor Climatic Change*, *Proceedings of NHRI Workshop No. 8*, National Hydrology Research Institute, Saskatoon, SK, 1992, pp. 57-78.

Helsel, D.R., and Hirsch, R.M., *Statistical Methods in Water Resources*, Elsevier Science Publishing, New York, 1992, p. 522.

Hershfield, D.M., "Rainfall Frequency Atlas of the United States for Durations from 30 Minutes to 24 Hours and Return Periods from 1 to 100 Years", U.S. Weather Bureau, Washington, D.C., Technical Paper 40, 1961.

Hirsch, R. M., Slack J. R., and Smith R. A., "Techniques of Trend Analysis for Monthly Water Quality Data", *Water Resources Research*, Vol. 18, 1982, pp. 107-121.

Huff, F.A., and Angel, J.R., *Frequency Distribution and Hydraulic Climatic Characteristics of Heavy Rainstorms in Illinois*, Bulletin 70, Illinois State Water Survey, Champaign, Illinois, U.S.A, 1989.

Huff, F.A., and Angel, J.R., *Rainfall Frequency Atlas of the Midwest*, Bulletin 71, Midwestern Climate Center and Illinois State Water Service, 1992, pp. 5-6.

*Hydrological Atlas of Canada*, Fisheries and Environment Canada, 1978, pp. 5-7.

IPCC, *Impacts, Adaptations and Mitigation of Climate Change: Scientific-Technical Analyses*, Cambridge University Press, UK, 1995, p. 878

IPCC, *Special Report on the Regional Impacts of Climate Change: an Assessment of Vulnerability*, Cambridge University Press, UK, 2001.

Kahya, E., and Kalaycı, S., "Trend Analysis of Streamflow in Turkey", *Journal of Hydrology*, Vol. 289, 2004, pp. 128-144.

Kendall, M.G., *Rank Correlation Measures*, Charles Griffin, London, 1975.

Kharin, V.V., and Zwiers F.W., "Changes in the Extremes in an Ensemble of Transient Climate Simulations with a Coupled Atmosphere-ocean GCM", *Journal of Climate*, Vol. 13, 2000, pp. 3760-3780.

Kije Sipi Ltd, "Impacts and Adaptation of Drainage Systems, Design Methods & Policies", Report Presented to Natural Resources Canada Climate Change Action Fund: Impacts & Adaptation, 2001.

Kistler, R., Kalnay, E., Collins, W., Saha, S., White, G., Woollen, J., Chelliah, M., Ebisuzaki, W., Kanamitsu, M., Kousky, V., Dool, H.v.d, Jenne, R., and Fiorino, M., "The NCEP/NCAR 50-year Reanalysis", *Bulletin of the American Meteorological Society*, Vol. 82, No. 2, 2001, pp. 247-267.

Mann, H.B., Non-parametric tests against trend, *Econometrica* 13, MathSciNet, 1945, pp. 245-259.

Marbek Resource Consultants, "Impact of Climate Change on Transportation in Canada, Transport Canada", Final Workshop Report, 2003.

Mekis, É., and Hogg, W.D., "Rehabilitation and Analysis of Canadian Daily Precipitation Time Series", *Atmosphere-Ocean*, Vol. 37, No. 1, 1999, pp. 53-85.

Morrison, J., Quick, M., Foreman, and M.G.G. "Climate change in the Fraser River watershed: flow and temperature projections", *Journal of Hydrology*, Vol. 263, 2002, pp. 230-244.

Watkins, D. W., "Design Storms for Stormwater Management in Michigan", *Proceedings of the ASCE/EWRI Water Resources Planning and Management Conference*, Roanoke, VA, May, 2002.

Wilby, R.L., Dawson, C.W., and Barrow, E.M., "SDSM - a Decision Support Tool for the Assessment of Regional Climate Change Impacts", *Environmental and Modelling Software*, Vol. 17, 2002, pp. 145-157.

Yue, S., Pilon, P., and Cavadias, G., "Power of the Mann-Kendall and Spearman's Rho Tests for Detecting Monotonic Trends in Hydrological Series", *Journal of Hydrology*, Vol. 259, 2002, pp. 254-271.

# Appendix

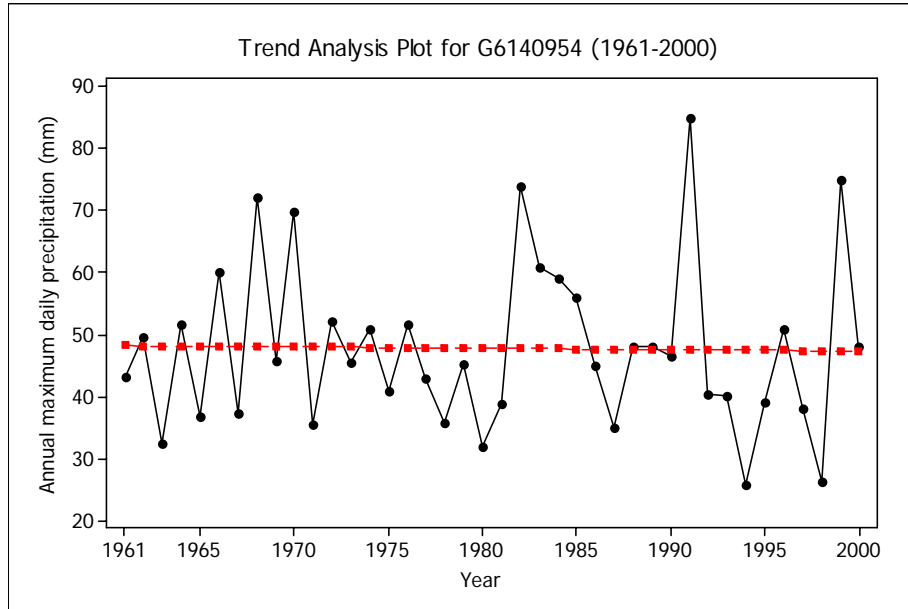


**Figure A1– Trend Analysis for Annual Maximum Daily Precipitation at Station G6140954 ( $p= 0.65$ )**

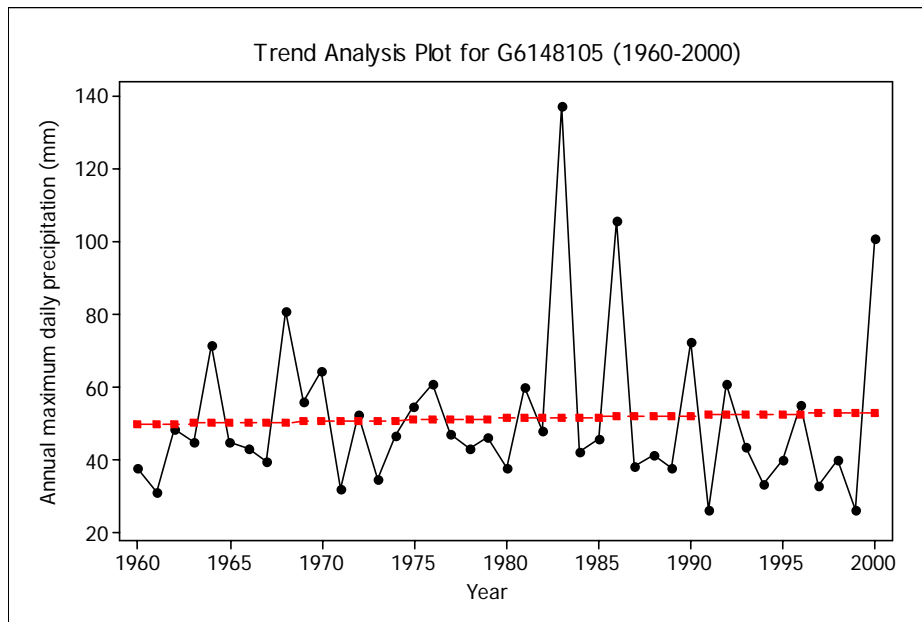


**Figure A2 – Trend Analysis for Annual Maximum Daily Precipitation at Station G6148105 ( $p= 0.44$ )**

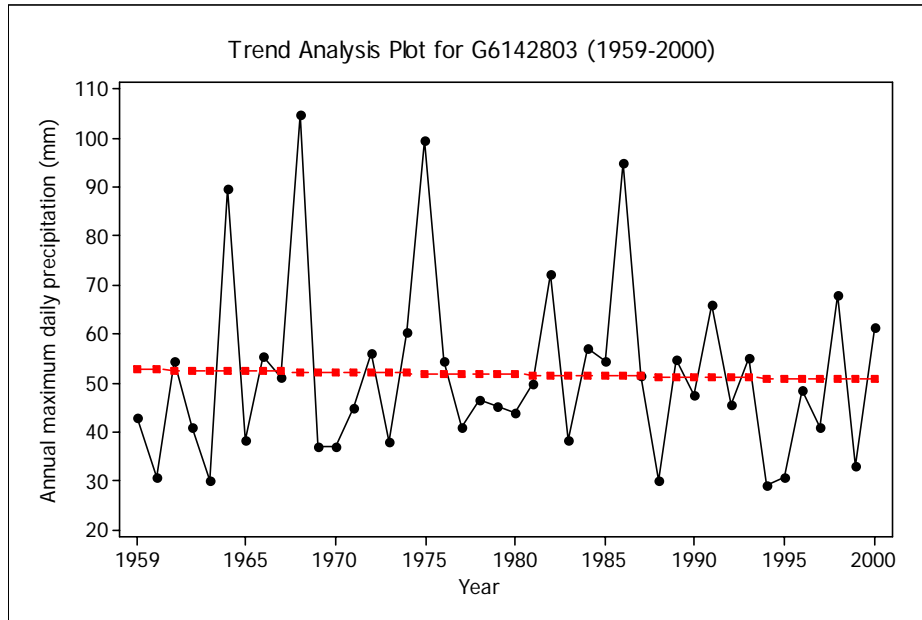


**Figure A3 – Trend Analysis for Annual Maximum Daily Precipitation at Station G6142803 ( $p= 0.63$ )**

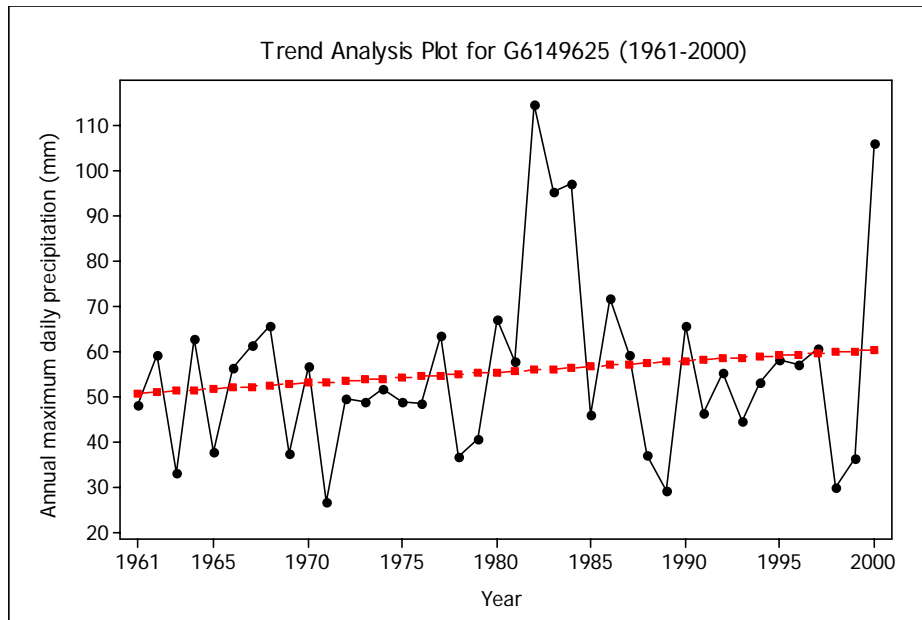


**Figure A4 – Trend Analysis for Annual Maximum Daily Precipitation at Station G6149625 ( $p= 0.68$ )**

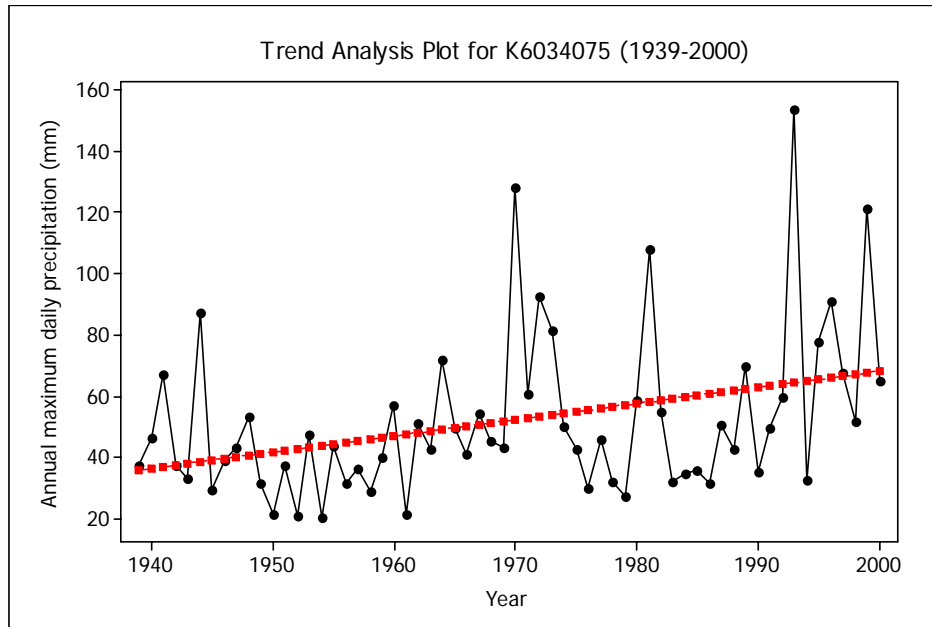


**Figure A5 – Trend Analysis for Annual Maximum Daily Precipitation at Station K6034075 ( $p= 0.006$ )**

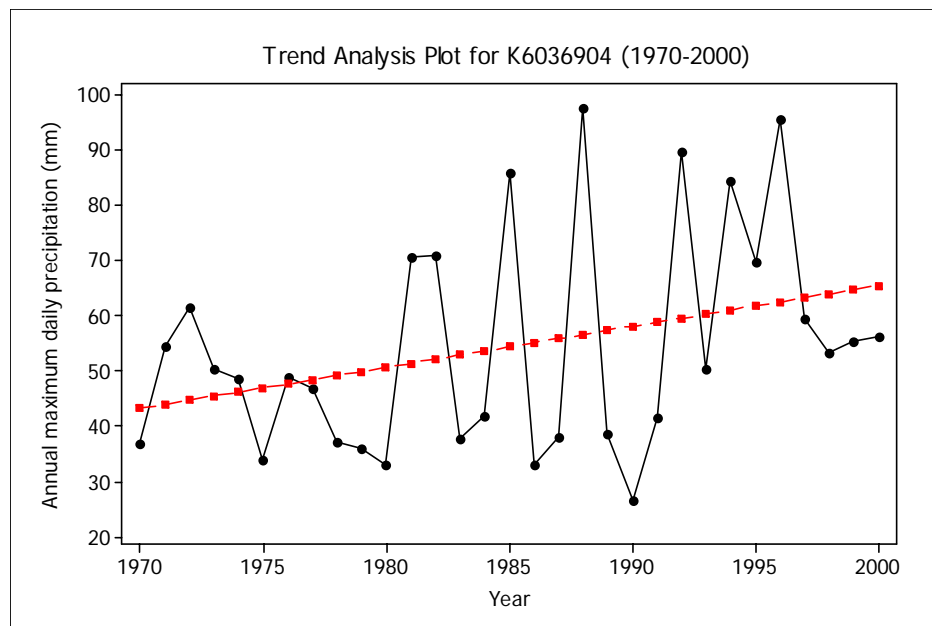


**Figure A6 – Trend Analysis for Annual Maximum Daily Precipitation at Station K6036904 ( $p= 0.1$ )**

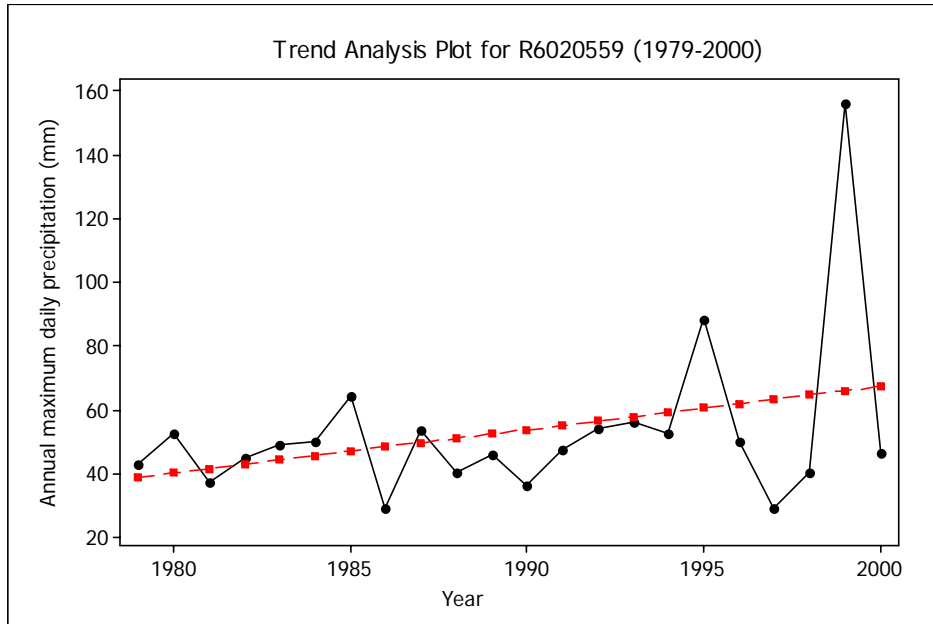


**Figure A7– Trend Analysis for Annual Maximum Daily Precipitation at Station R6020559 ( $p= 0.31$ )**

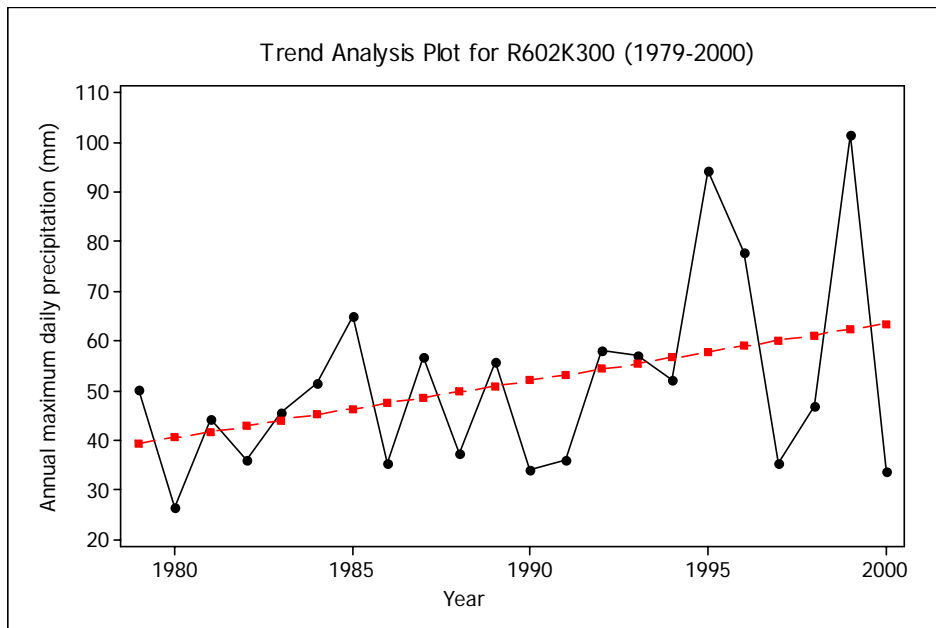


**Figure A8 – Trend Analysis for Annual Maximum Daily Precipitation at Station R602K300 ( $p= 0.21$ )**

**Table A1 – Observed Precipitation (1961-1980): Precipitation Intensity for Different Return Periods at Station G6140954**

	T=2 years	T=5 years	T=10 years	T=20 years	T=50 years	T=100 years
$T_d$ (hr)						
	(mm/hr)	(mm/hr)	(mm/hr)	(mm/hr)	(mm/hr)	(mm/hr)
<b>24</b>	2.1	2.6	2.9	3.2	3.6	3.9
<b>18</b>	2.6	3.1	3.5	3.9	4.4	4.7
<b>12</b>	3.5	4.2	4.8	5.3	5.9	6.4
<b>6</b>	6.2	7.6	8.5	9.4	10.5	11.4
<b>3</b>	10.8	13.3	14.9	16.4	18.4	19.9
<b>2</b>	14.2	17.4	19.5	21.6	24.2	26.2
<b>1</b>	22.8	28.0	31.4	34.7	38.9	42.1
<b>0.5</b>	38.5	47.2	53.0	58.5	65.7	71.1
<b>0.25</b>	58.8	72.1	80.9	89.3	100.3	108.4
<b>0.17</b>	65.6	80.4	90.2	99.7	111.8	121.0
<b>0.08</b>	76.0	93.2	104.6	115.5	129.6	140.2

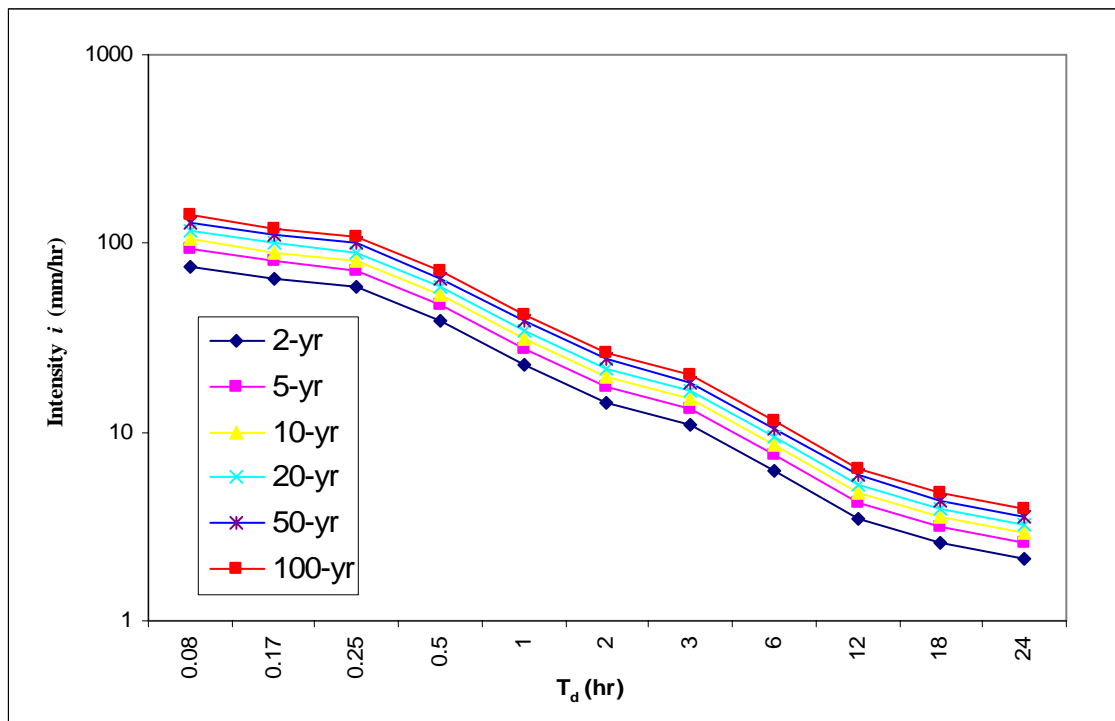


**Figure A9 – IDF Curves for Observed Precipitation (1961-1980) at Station G6140954**

**Table A2 – Observed Precipitation (1981-2000): Precipitation Intensity for Different Return Periods at Station G6140954**

$T_d$ (hr)	T=2 years	T=5 years	T=10 years	T=20 years	T=50 years	T=100 years
	(mm/hr)	(mm/hr)	(mm/hr)	(mm/hr)	(mm/hr)	(mm/hr)
24	2.2	2.9	3.3	3.7	4.3	4.7
18	2.7	3.5	4.0	4.5	5.2	5.7
12	3.6	4.7	5.4	6.1	7.0	7.7
6	6.5	8.4	9.7	10.9	12.5	13.7
3	11.3	14.7	16.9	19.1	21.9	23.9
2	14.8	19.3	22.2	25.0	28.7	31.4
1	23.9	31.0	35.7	40.3	46.1	50.5
0.5	40.3	52.4	60.3	68.0	77.9	85.3
0.25	61.5	79.9	92.1	103.8	118.9	130.2
0.17	68.6	89.2	102.7	115.8	132.6	145.3
0.08	79.6	103.3	119.1	134.2	153.7	168.4

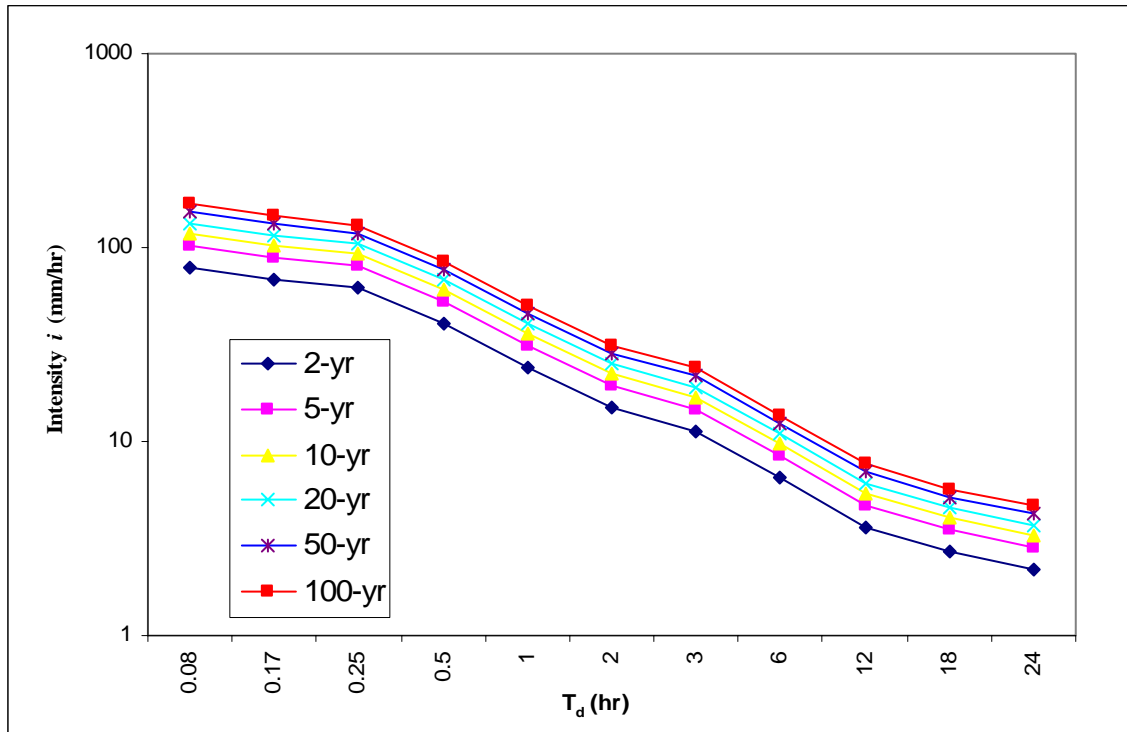


**Figure A10 – IDF Curves for Observed Precipitation (1981-2000) at Station G6140954**

**Table A3 – Observed Precipitation (1960-1980): Precipitation Intensity for Different Return Periods at Station G6148105**

	T=2 years	T=5 years	T=10 years	T=20 years	T=50 years	T=100 years
$T_d$ (hr)						
	(mm/hr)	(mm/hr)	(mm/hr)	(mm/hr)	(mm/hr)	(mm/hr)
24	2.3	2.8	3.1	3.4	3.9	4.2
18	2.7	3.4	3.8	4.2	4.7	5.1
12	3.7	4.5	5.1	5.7	6.4	6.9
6	6.6	8.1	9.1	10.1	11.3	12.2
3	11.5	14.2	16.0	17.6	19.8	21.5
2	15.1	18.6	20.9	23.2	26.0	28.2
1	24.3	29.9	33.7	37.2	41.8	45.3
0.5	41.1	50.6	56.9	62.9	70.6	76.5
0.25	62.7	77.2	86.8	96.0	107.8	116.7
0.17	70.0	86.1	96.8	107.0	120.3	130.2
0.08	81.1	99.8	112.2	124.1	139.4	151.0

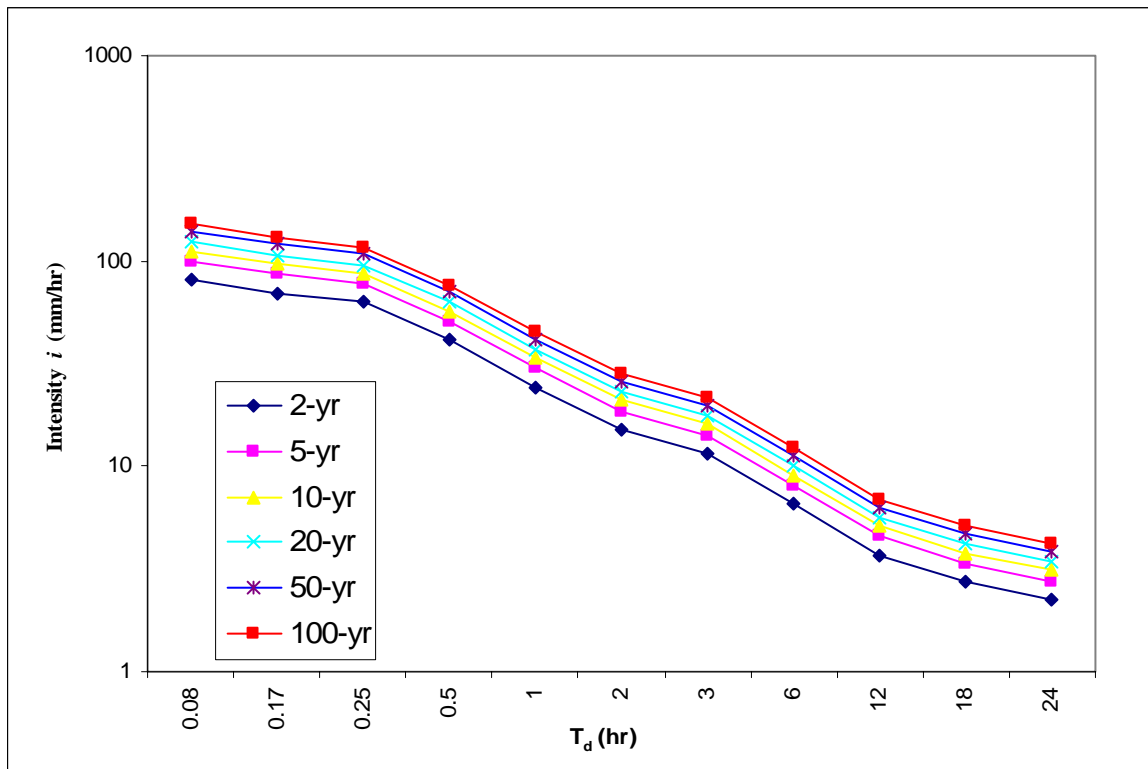


**Figure A11– IDF curves for Observed Precipitation (1960-1980) at Station G6148105**

**Table A4 – Observed Precipitation (1981-2000): Precipitation Intensity for Different Return Periods at Station G6148105**

$T_d$ (hr)	T=2 years	T=5 years	T=10 years	T=20 years	T=50 years	T=100 years
	(mm/hr)	(mm/hr)	(mm/hr)	(mm/hr)	(mm/hr)	(mm/hr)
24	2.3	3.6	4.4	5.2	6.2	7.0
18	2.8	4.3	5.3	6.3	7.5	8.4
12	3.8	5.8	7.2	8.5	10.2	11.4
6	6.8	10.4	12.8	15.1	18.1	20.3
3	11.9	18.2	22.5	26.5	31.7	35.7
2	15.6	23.9	29.5	34.8	41.7	46.8
1	25.1	38.5	47.4	55.9	66.9	75.2
0.5	42.3	65.0	80.0	94.4	113.1	127.0
0.25	64.6	99.2	122.1	144.1	172.6	193.9
0.17	72.1	110.7	136.3	160.8	192.5	216.3
0.08	83.5	128.3	157.9	186.4	223.1	250.7

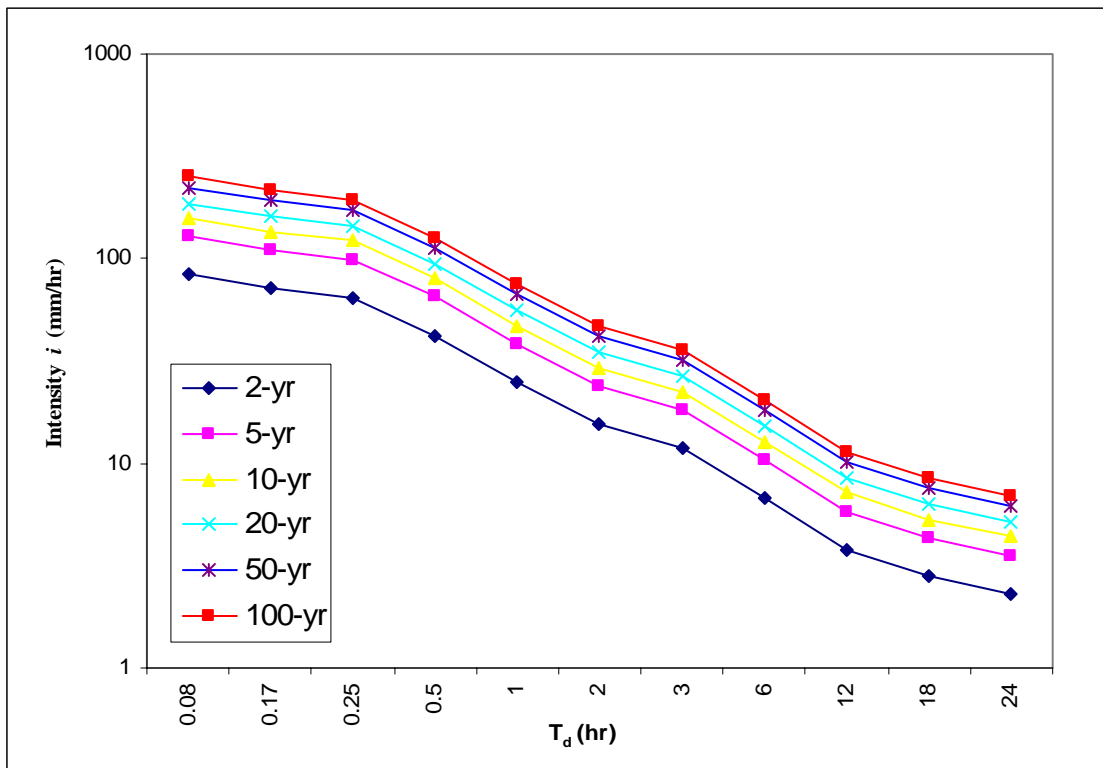


**Figure A12 – IDF Curves for Observed Precipitation (1981-2000) at Station G6148105**

**Table A5 – Observed Precipitation (1959-1979): Precipitation Intensity for Different Return Periods at Station G6142803**

	T=2 years	T=5 years	T=10 years	T=20 years	T=50 years	T=100 years
T <sub>d</sub> (hr)	(mm/hr)	(mm/hr)	(mm/hr)	(mm/hr)	(mm/hr)	(mm/hr)
24	2.3	3.2	3.8	4.4	5.1	5.7
18	2.8	3.9	4.6	5.3	6.2	6.9
12	3.8	5.3	6.2	7.2	8.4	9.3
6	6.8	9.4	11.1	12.8	14.9	16.5
3	11.9	16.4	19.5	22.4	26.1	29.0
2	15.6	21.6	25.6	29.4	34.3	38.0
1	25.0	34.7	41.1	47.2	55.1	61.1
0.5	42.3	58.6	69.4	79.7	93.1	103.1
0.25	64.6	89.4	105.9	121.7	142.1	157.4
0.17	72.0	99.8	118.1	135.7	158.5	175.6
0.08	83.5	115.6	136.9	157.3	183.8	203.6

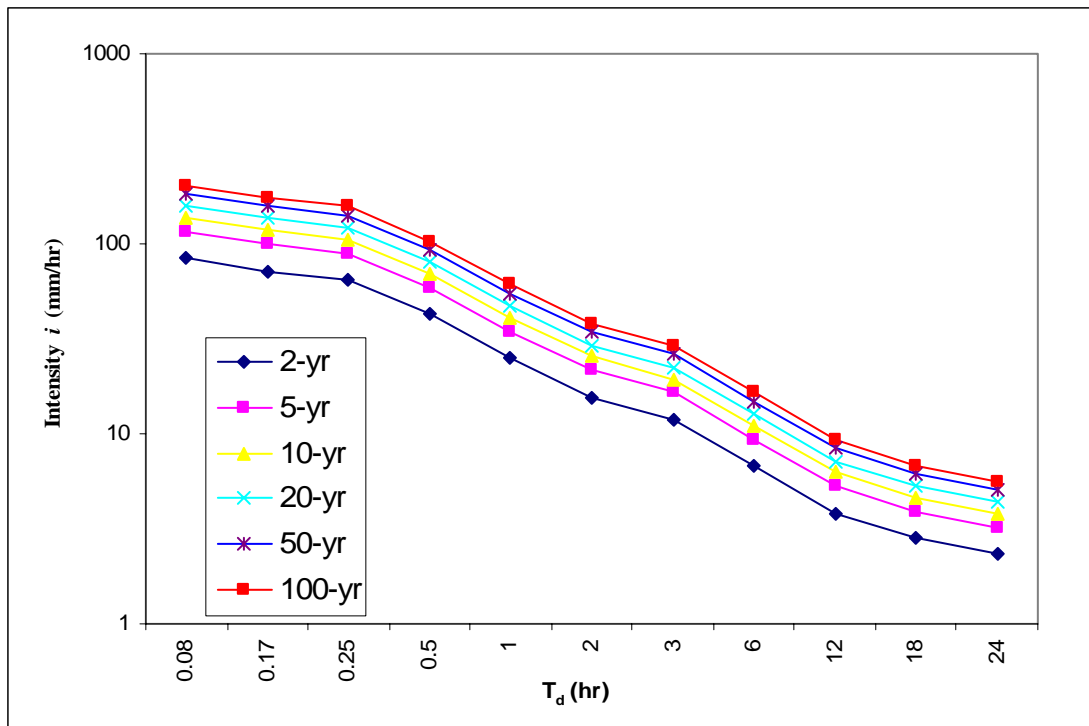


**Figure A13 – IDF Curves for Observed Precipitation (1959-1979) at Station G6142803**

**Table A6 – Observed Precipitation (1980-2000): Precipitation Intensity for Different Return Periods at Station G6142803**

$T_d$ (hr)	T=2 years	T=5 years	T=10 years	T=20 years	T=50 years	T=100 years
	(mm/hr)	(mm/hr)	(mm/hr)	(mm/hr)	(mm/hr)	(mm/hr)
24	2.3	3.0	3.4	3.9	4.4	4.8
18	2.8	3.6	4.2	4.7	5.4	5.9
12	3.8	4.9	5.6	6.3	7.2	7.9
6	6.7	8.7	10.0	11.3	12.9	14.1
3	11.8	15.2	17.5	19.7	22.6	24.8
2	15.4	20.0	23.0	25.9	29.7	32.5
1	24.8	32.1	37.0	41.7	47.7	52.2
0.5	41.9	54.3	62.5	70.4	80.5	88.2
0.25	63.9	82.8	95.4	107.4	122.9	134.6
0.17	71.3	92.4	106.4	119.8	137.2	150.2
0.08	82.6	107.1	123.3	138.8	159.0	174.0

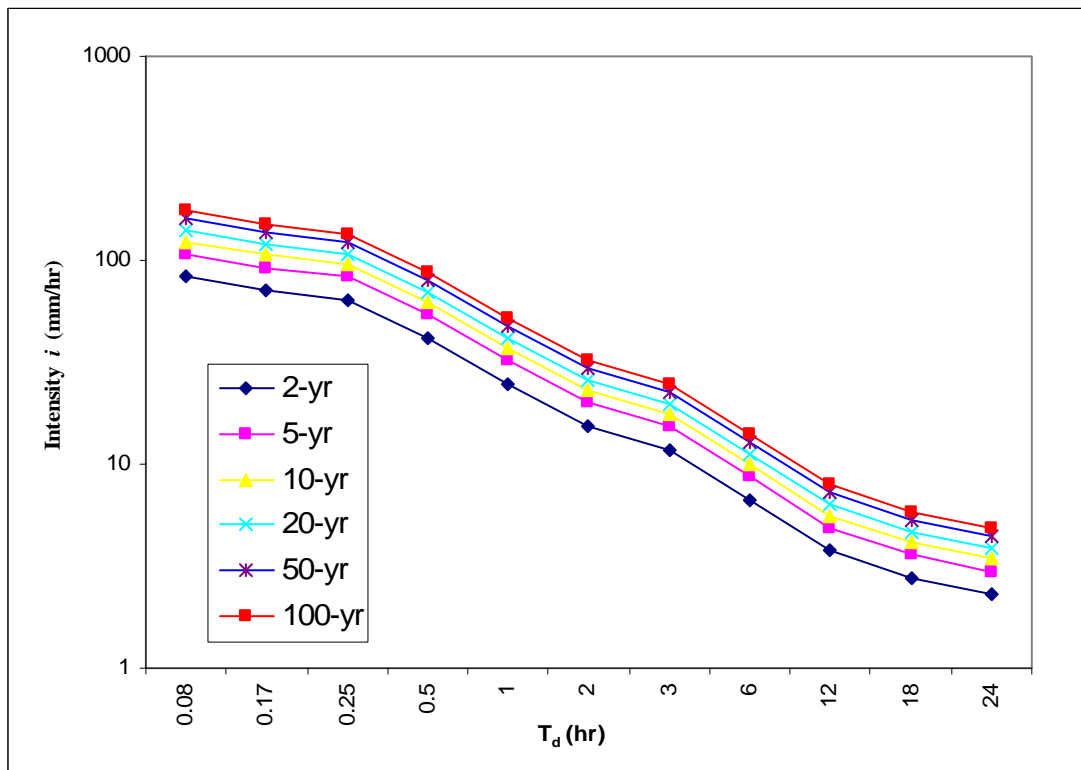


**Figure A14 – IDF Curves for Observed Precipitation (1980-2000) at Station G6142803**

**Table A7 – Observed Precipitation (1961-1980): Precipitation Intensity for Different Return Periods at Station G6149625**

	T=2 years	T=5 years	T=10 years	T=20 years	T=50 years	T=100 years
T <sub>d</sub> (hr)	(mm/hr)	(mm/hr)	(mm/hr)	(mm/hr)	(mm/hr)	(mm/hr)
24	2.3	2.7	3.1	3.4	3.8	4.1
18	2.7	3.3	3.7	4.1	4.6	4.9
12	3.7	4.5	5.0	5.5	6.2	6.7
6	6.6	8.0	8.9	9.8	11.0	11.9
3	11.5	14.0	15.7	17.3	19.3	20.8
2	15.2	18.4	20.6	22.7	25.3	27.4
1	24.4	29.6	33.1	36.4	40.7	44.0
0.5	41.1	50.0	55.9	61.5	68.8	74.3
0.25	62.8	76.3	85.3	93.9	105.0	113.3
0.17	70.1	85.2	95.2	104.7	117.1	126.4
0.08	81.2	98.7	110.3	121.4	135.8	146.6

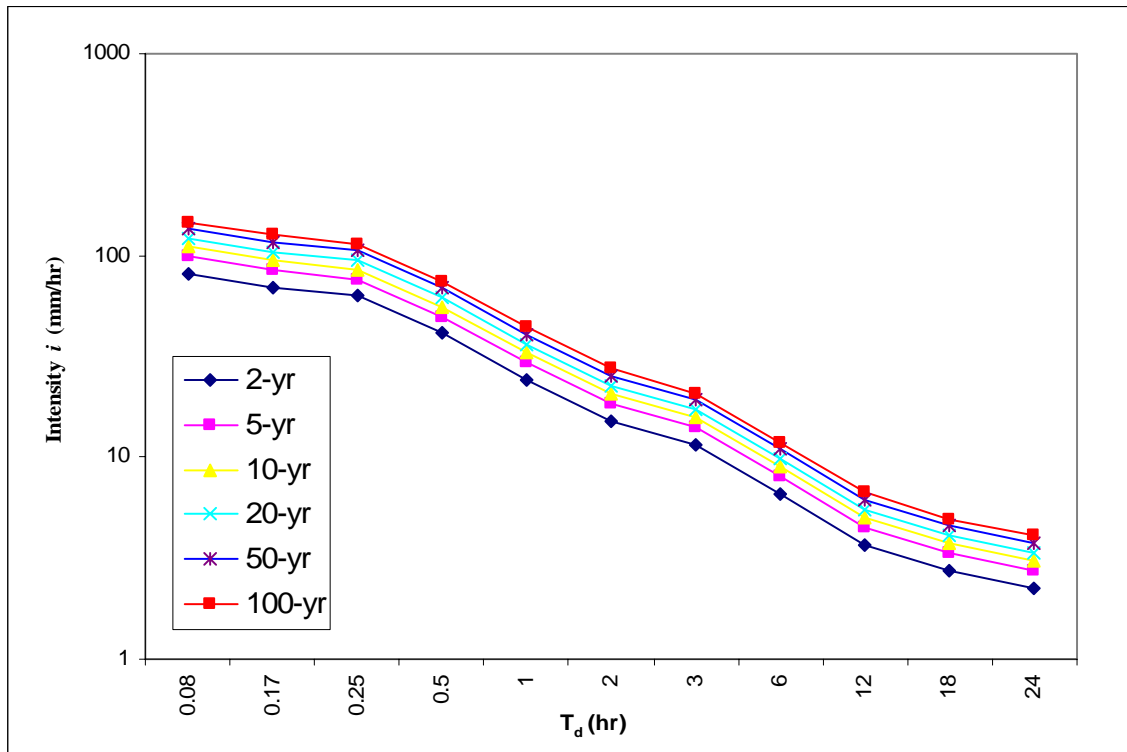


**Figure A15 – IDF curves for Observed Precipitation (1961-1980) at Station G61499625**

**Table A8 – Observed Precipitation (1981-2000): Precipitation Intensity for Different Return Periods at Station G6149625**

$T_d$ (hr)	T=2 years	T=5 years	T=10 years	T=20 years	T=50 years	T=100 years
	(mm/hr)	(mm/hr)	(mm/hr)	(mm/hr)	(mm/hr)	(mm/hr)
24	2.7	3.7	4.4	5.0	5.9	6.5
18	3.2	4.5	5.3	6.1	7.1	7.9
12	4.4	6.1	7.2	8.2	9.6	10.7
6	7.8	10.8	12.8	14.7	17.1	19.0
3	13.7	18.9	22.4	25.7	30.1	33.3
2	18.0	24.9	29.4	33.8	39.5	43.7
1	28.9	40.0	47.3	54.3	63.4	70.2
0.5	48.8	67.5	79.8	91.7	107.1	118.6
0.25	74.5	103.0	121.9	140.0	163.4	181.0
0.17	83.1	114.9	136.0	156.2	182.3	201.9
0.08	96.3	133.2	157.6	181.0	211.3	234.1

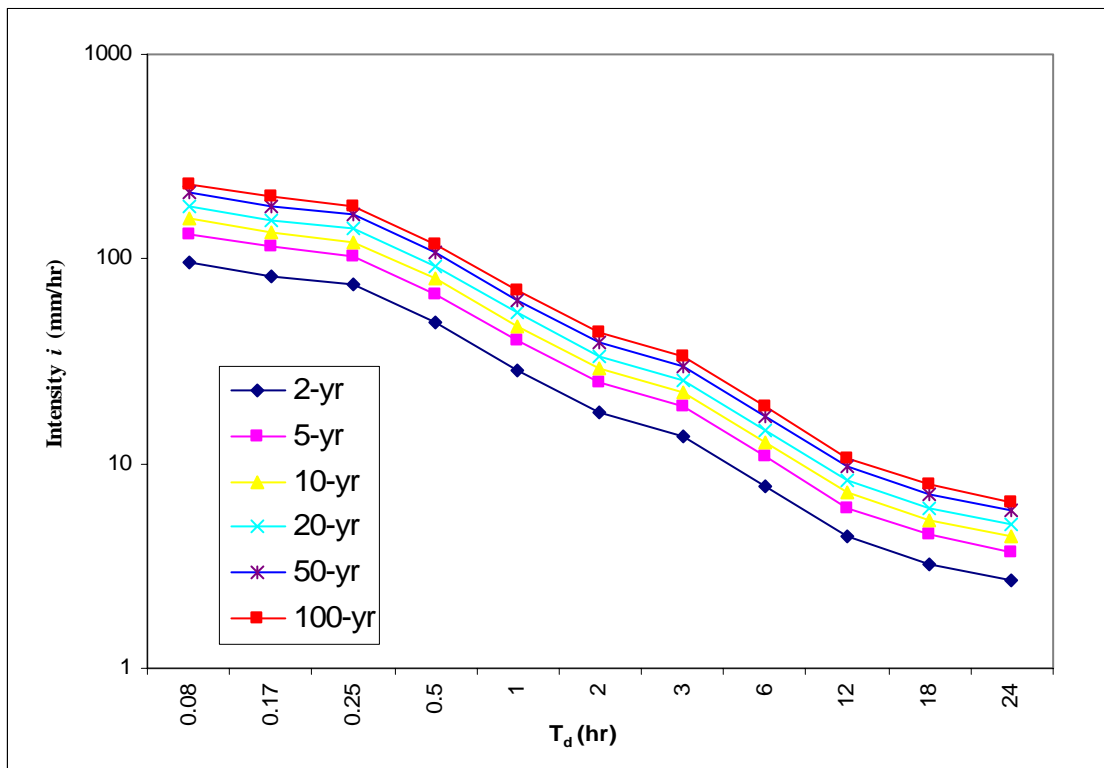


**Figure A16 – IDF Curves for Observed Precipitation (1981-2000) at Station G6149625**

**Table A9 – Current and predicted rainfall intensity and percentage of increase (in parentheses) at station G6140954**

Return Period (years)	Climate Conditions	Rainfall Duration (hours)							
		24	18	12	6	3	2	1	0.5
	Current	2.1	2.6	3.5	6.3	11.0	14.4	23.2	39.2
2-yr	2050s (%Increase)	2.4(14)	2.9(12)	3.9(11)	6.9(10)	12.1(10)	15.9(10)	25.5(10)	43.1(10)
	2080s (%Increase)	2.6(24)	3.2(23)	4.3(23)	7.6(21)	13.3(21)	17.5(22)	28.1(21)	47.5(21)
	Current	2.7	3.3	4.5	7.9	13.9	18.3	29.3	49.6
5-yr	2050s (%Increase)	3.3(22)	4.0(21)	5.4(20)	9.6(22)	16.8(21)	22.0(20)	35.4(21)	59.8(21)
	2080s (%Increase)	3.7(37)	4.5(36)	6.1(36)	10.8(37)	18.9(36)	24.9(36)	40.0(37)	67.5(36)
	Current	3.1	3.8	5.1	9.0	15.8	20.8	33.4	56.4
10-yr	2050s (%Increase)	3.9(26)	4.7(24)	6.4(25)	11.4(27)	19.9(26)	26.1(25)	42.0(26)	70.9(26)
	2080s (%Increase)	4.4(42)	5.4(42)	7.3(43)	12.9(43)	22.7(44)	29.7(43)	47.8(43)	80.7(43)
	Current	3.5	4.2	5.7	10.1	17.7	23.2	37.3	63.0
20-yr	2050s (%Increase)	4.5(29)	5.4(29)	7.3(28)	13.0(29)	22.9(29)	30.0(29)	48.3(29)	81.5(29)
	2080s (%Increase)	5.1(46)	6.2(48)	8.4(47)	15.0(49)	26.2(48)	34.4(48)	55.3(48)	93.4(48)
	Current	3.9	4.8	6.4	11.4	20.1	26.3	42.3	71.5
50-yr	2050s (%Increase)	5.2(33)	6.3(31)	8.6(34)	15.2(33)	26.7(33)	35.1(33)	56.4(33)	95.3(33)
	2080s (%Increase)	6.0(54)	7.3(52)	9.9(55)	17.6(54)	30.8(53)	40.5(54)	65.1(54)	109.9(54)
	Current	4.3	5.2	7.0	12.5	21.9	28.7	46.1	77.9
100-yr	2050s (%Increase)	5.8(35)	7.0(35)	9.5(36)	16.9(35)	29.6(35)	38.9(35)	62.5(35)	105.5(35)
	2080s (%Increase)	6.7(56)	8.1(56)	11.0(57)	19.6(57)	34.3(57)	45.0(57)	72.3(57)	122.2(57)

**Table A10 – Current and predicted rainfall intensity and percentage of increase (in parentheses) at station G6148105.**

Return Period (years)	Climate Conditions	Rainfall Duration (hours)							
		24	18	12	6	3	2	1	0.5
	Current	2.3	2.8	3.8	6.7	11.7	15.4	24.7	41.7
2-yr	2050s (%Increase)	2.5 (9)	3.1 (11)	4.1(8)	7.4 (10)	12.9 (10)	17(10)	27.3 (11)	46 (10)
	2080s (%Increase)	2.5 (9)	3 (7)	4 (5)	7.2 (7)	12.6 (8)	16.5 (7)	26.5 (7)	44.8 (7)
	Current	3.2	3.9	5.3	9.4	16.5	21.6	34.8	58.7
5-yr	2050s (%Increase)	3.6 (13)	4.4(13)	5.9(11)	10.6(13)	18.6(13)	24.4(13)	39.2(13)	66.1(13)
	2080s (%Increase)	3.7(16)	4.5(15)	6.1(15)	10.9(16)	19.1(16)	25(16)	40.2(16)	67.9(16)
	Current	3.8	4.7	6.3	11.2	19.7	25.8	41.4	70.0
10-yr	2050s (%Increase)	4.4(16)	5.3(13)	7.1(13)	12.7(13)	22.3(13)	29.3(14)	47(14)	79.5(14)
	2080s (%Increase)	4.6 (21)	5.5(17)	7.5(19)	13.3(19)	23.4(19)	30.7(19)	49.3(19)	83.2(19)
	Current	4.4	5.4	7.3	12.9	22.7	29.8	47.8	80.8
20-yr	2050s (%Increase)	5.1(16)	6.1(13)	8.3(14)	14.8(15)	25.9(14)	34(14)	54.6(14)	92.2(14)
	2080s (%Increase)	5.4(23)	6.5(20)	8.8 (21)	15.7(22)	27.5(21)	36.1(21)	58(21)	97.9(21)
	Current	5.2	6.3	8.5	15.2	26.6	34.9	56.1	94.8
50-yr	2050s (%Increase)	6(15)	7.2(14)	9.8(15)	17.4(14)	30.5(15)	40.1(15)	64.4(15)	108.8(15)
	2080s (%Increase)	6.4 (23)	7.8 (24)	10.5(24)	18.7(23)	32.8(23)	43.1(23)	69.2(23)	116.9(23)
	Current	5.8	7.0	9.5	16.9	29.6	38.8	62.3	105.3
100-yr	2050s (%Increase)	6.6 (14)	8.1(16)	10.9(15)	19.4(15)	34(15)	44.6(15)	71.7(15)	121.2(15)
	2080s (%Increase)	7.2 (24)	8.7(24)	11.8(24)	21(24)	36.8(24)	48.3(24)	77.7(25)	131.2(25)

**Table A11– Current and predicted rainfall intensity and percentage of increase (in parentheses) at station G6142803**

Return Period (years)	Climate Conditions	Rainfall Duration (hours)							
		24	18	12	6	3	2	1	0.5
	Current	2.3	2.8	3.8	6.7	11.8	15.5	24.8	41.9
2-yr	2050s (%Increase)	2.2 (-4)	2.6(-7)	3.6(-5)	6.3(-6)	11.1(-6)	14.6(-6)	23.4(-6)	39.5(-6)
	2080s (%Increase)	2.1(-9)	2.5(-11)	3.4(-11)	6.1(-9)	10.6(-10)	14(-10)	22.5(-9)	37.9(-10)
	Current	3.1	3.7	5	9	15.7	20.7	33.2	56.1
5-yr	2050 s(%Increase)	2.8(-10)	3.4(-8)	4.6(-8)	8.2(-9)	14.4(-8)	18.8(-9)	30.3(-9)	51.1(-9)
	2080s (%Increase)	2.8(-10)	3.4(-8)	4.6(-8)	8.3(-8)	14.5(-8)	19(-8)	30.6(-8)	51.6(-8)
	Current	3.6	4.4	5.9	10.5	18.4	24.1	38.8	65.5
10-yr	2050s (%Increase)	3.2(-11)	3.9(-11)	5.3(-10)	9.4(-10)	16.5(-10)	21.7(-10)	34.8(-10)	58.8(-10)
	2080s (%Increase)	3.3(-8)	4(-9)	5.5(-7)	9.7(-8)	17(-8)	22.4(-7)	35.9(-7)	60.7(-7)
	Current	4.1	5	6.7	11.9	20.9	27.4	44.1	74.5
20-yr	2050s (%Increase)	3.6(-12)	4.4(-12)	6(-10)	10.6(-11)	18.6(-11)	24.4(-11)	39.2(-11)	66.2(-11)
	2080s (%Increase)	3.8(-7)	4.6(-8)	6.2(-7)	11.1(-7)	19.5(-7)	25.6(-7)	41.1(-7)	69.4(-7)
	Current	4.7	5.7	7.7	13.8	24.2	31.7	51	86.1
50-yr	2050s (%Increase)	4.2(-11)	5(-12)	6.8(-12)	12.1(-12)	21.3(-12)	27.9(-12)	44.8(-12)	75.7(-12)
	2080s (%Increase)	4.4(-6)	5.4(-5)	7.2(-6)	12.9(-7)	22.6(-7)	29.7(-6)	47.7(-6)	80.6(-6)
	Current	5.2	6.3	8.5	15.2	26.6	34.9	56.1	94.8
100-yr	2050s (%Increase)	4.5(-13)	5.5(-13)	7.5(-12)	13.3(-13)	23.3(-12)	30.5(-13)	49.1(-12)	82.9(-13)
	2080s (%Increase)	4.9(-6)	5.9(-6)	8(-6)	14.3(-6)	25(-6)	32.8(-6)	52.7(-6)	89(-6)

**Table A12 – Current and predicted rainfall intensity and percentage of increase (in parentheses) at station G6149625**

Return Period (years)	Climate Conditions	Rainfall Duration (hours)							
		24	18	12	6	3	2	1	0.5
	Current	2.5	3	4	7.2	12.6	16.5	26.5	44.7
2-yr	2050s(%Increase)	2.3(-8)	2.8(-7)	3.7(-8)	6.6(-8)	11.7(-7)	15.3(-7)	24.6(-7)	41.5(-7)
	2080s (%Increase)	2.5(0)	3.1(3)	4.1(3)	7.3(1)	12.9(2)	16.9(2)	27.2(3)	45.9(3)
	Current	3.3	4	5.4	9.6	16.8	22	35.4	59.8
5-yr	2050s (%Increase)	3.5(6)	4.3(8)	5.8(7)	10.2(6)	18(7)	23.6(7)	37.9(7)	64(7)
	2080s (%Increase)	3.9 (18)	4.7(18)	6.4(19)	11.4(19)	20(19)	26.3(20)	42.2(19)	71.3(19)
	Current	3.8	4.6	6.3	11.2	19.6	25.7	41.3	69.7
10-yr	2050s (%Increase)	4.3(13)	5.2(13)	7.1(13)	12.6(13)	22.1(13)	29.1(13)	46.7(13)	78.9(13)
	2080s (%Increase)	4.8(26)	5.9(28)	7.9(25)	14.1(26)	24.8(27)	32.5(26)	52.2(26)	88.2(27)
	Current	4.3	5.3	7.1	12.7	22.3	29.2	46.9	79.3
20-yr	2050s (%Increase)	5.1(19)	6.2(17)	8.4(18)	14.9(17)	26.1(17)	34.3(17)	55.1(17)	93.1(17)
	2080s (%Increase)	5.7(33)	6.9(30)	9.4(32)	16.7(31)	29.3(31)	38.5(32)	61.8(32)	104.4(32)
	Current	5	6.1	8.2	14.7	25.7	33.8	54.3	91.7
50-yr	2050s (%Increase)	6.1(22)	7.4(21)	10(22)	17.9(22)	31.3(22)	41.1(22)	66.1(22)	111.6(22)
	2080s (%Increase)	6.9(38)	8.3(36)	11.3(38)	20.1(37)	35.2(37)	46.2(37)	74.2(37)	125.3(37)
	Current	5.5	6.7	9.1	16.2	28.3	37.2	59.8	100.9
100-yr	2050s (%Increase)	6.9(25)	8.3(24)	11.3(24)	20.1(24)	35.2(24)	46.2(24)	74.3(24)	125.4(24)
	2080s (%Increase)	7.7(40)	9.4(40)	12.7(40)	22.6(40)	39.6(40)	52(40)	83.5(40)	141(40)

**Table A13 – Current and predicted rainfall intensity and percentage of increase (in parentheses) at station K6034075**

Return Period (years)	Climate Conditions	Rainfall Duration (hours)							
		24	18	12	6	3	2	1	0.5
	Current	2.5	3.1	4.1	7.4	12.9	16.9	27.2	45.9
2-yr	2050s (%Increase)	2.8 (12)	3.4(10)	4.5(10)	8.1(9)	14.2(10)	18.6(10)	29.9(10)	50.5(10)
	2080s (%Increase)	3.2(28)	3.9(26)	5.2(27)	9.3(26)	16.4(27)	21.5(27)	34.6(27)	58.4(27)
	Current	3.7	4.5	6.1	10.9	19.1	25.1	40.4	68.2
5-yr	2050s (%Increase)	4.4(19)	5.3(18)	7.2(18)	12.8(17)	22.4(17)	29.4(17)	47.3(17)	79.8(17)
	2080s (%Increase)	5.0(35)	6.1(36)	8.2(34)	14.6(34)	25.7(35)	33.7(34)	54.2(34)	91.5(34)
	Current	4.5	5.5	7.5	13.3	23.3	30.6	49.1	82.9
10-yr	2050s (%Increase)	5.4(20)	6.6(20)	8.9(19)	15.9(20)	27.8(19)	36.6(20)	58.7(20)	99.2(20)
	2080s (%Increase)	6.2(38)	7.5(36)	10.2(36)	18.2(37)	31.8(36)	41.8(37)	67.2(37)	113.4(37)
	Current	5.3	6.5	8.7	15.5	27.2	35.8	57.5	97.1
20-yr	2050s (%Increase)	6.5(23)	7.8(20)	10.6(22)	18.9(22)	33.1(22)	43.4(21)	69.8(21)	117.8(21)
	2080s (%Increase)	7.4(40)	8.9(37)	12.1(39)	21.5(39)	37.8(39)	49.5(38)	79.6(38)	134.5(39)
	Current	6.3	7.7	10.4	18.5	32.4	42.5	68.3	115.4
50-yr	2050s (%Increase)	7.8(24)	9.4(22)	12.8(23)	22.7(23)	39.8(23)	52.3(23)	84(23)	141.9(23)
	2080s (%Increase)	8.9(41)	10.8(40)	14.5(39)	25.9(40)	45.4(40)	59.6(40)	95.8(40)	161.7(40)
	Current	7.1	8.6	11.6	20.7	36.2	47.6	76.4	129.1
100-yr	2050 s(%Increase)	8.8(24)	10.6(23)	14.4(24)	25.6(24)	44.9(24)	58.9(24)	94.7(24)	160(24)
	2080s (%Increase)	10.0(41)	12.1(41)	16.4(41)	29.2(41)	51.1(41)	67.1(41)	107.8(41)	182.1(41)

**Table A14 – Current and predicted rainfall intensity and percentage of increase (in parentheses) at station K6036904**

Return Period (years)	Climate Conditions	Rainfall Duration (hours)							
		24	18	12	6	3	2	1	0.5
	Current	2.4	2.9	3.9	7	12.3	16.2	26	43.8
2-yr	2050s (%Increase)	2.2(-8)	2.7(-7)	3.6(-8)	6.4(-9)	11.3(-8)	14.8(-9)	23.8(-8)	40.2(-8)
	2080s (%Increase)	2.3(-4)	2.8(-3)	3.7(-5)	6.6(-6)	11.6(-6)	15.3(-6)	24.5(-6)	41.4(-5)
	Current	3.2	3.9	5.3	9.4	16.5	21.7	34.9	59
5-yr	2050s(%Increase)	3.4(6)	4.1(5)	5.6(6)	9.9(5)	17.4(5)	22.8(5)	36.7(5)	62(5)
	2080s (%Increase)	3.6(13)	4.3(10)	5.9(11)	10.4(11)	18.3(11)	24(11)	38.6(11)	65.1(10)
	Current	3.8	4.6	6.2	11	19.4	25.4	40.8	69
10-yr	2050s (%Increase)	4.2(11)	5.1(11)	6.9(11)	12.2(11)	21.5(11)	28.2(11)	45.3(11)	76.4(11)
	2080s (%Increase)	4.4(16)	5.4(17)	7.3(18)	12.9(17)	22.7(17)	29.8(17)	47.8(17)	80.8(17)
	Current	4.3	5.2	7.1	12.6	22.1	28.9	46.5	78.6
20-yr	2050s (%Increase)	4.9(14)	6(15)	8.1(14)	14.5(15)	25.3(14)	33.3(15)	53.5(15)	90.3(15)
	2080s (%Increase)	5.3(23)	6.4(23)	8.6(21)	15.3(21)	26.9(22)	35.3(22)	56.7(22)	95.8(22)
	Current	5	6.1	8.2	14.6	25.5	33.5	53.9	91
50-yr	2050 s(%Increase)	5.9(18)	7.2(18)	9.7(18)	17.3(18)	30.4(19)	39.9(19)	64.1(19)	108.2(19)
	2080s (%Increase)	6.3(26)	7.7(26)	10.4(27)	18.5(27)	32.4(27)	42.5(27)	68.3(27)	115.3(27)
	Current	5.5	6.7	9	16.1	28.2	37	59.4	100.3
100-yr	2050s (%Increase)	6.7(22)	8.1(21)	10.9(21)	19.5(21)	34.1(21)	44.8(21)	72(21)	121.6(21)
	2080s (%Increase)	7.1(29)	8.6(28)	11.7(30)	20.8(29)	36.5(29)	47.9(29)	76.9(29)	129.9(30)

**Table A15 – Current and predicted rainfall intensity and percentage of increase (in parentheses) at station R6020559**

Return Period (years)	Climate Conditions	Rainfall Duration (hours)							
		24	18	12	6	3	2	1	0.5
	Current	2.4	2.9	3.9	7	12.3	16.2	26	43.9
2-yr	2050s (%Increase)	2.4(0)	2.9(0)	3.9(0)	7(0)	12.2(-1)	16.1(-1)	25.8(-1)	43.6(-1)
	2080s (%Increase)	2.8(17)	3.4(17)	4.7(21)	8.3(19)	14.5(18)	19.1(18)	30.7(18)	51.8(18)
	Current	3.6	4.3	5.8	10.4	18.2	23.9	38.4	64.9
5-yr	2050s (%Increase)	3.9(8)	4.8(12)	6.5(12)	11.5(11)	20.2(11)	26.5(11)	42.6(11)	71.9(11)
	2080s (%Increase)	4.4(22)	5.3(23)	7.2(24)	12.9(24)	22.6(24)	29.6(24)	47.6(24)	80.4(24)
	Current	4.3	5.2	7.1	12.6	22.1	29	46.6	78.7
10-yr	2050s (%Increase)	5(16)	6(15)	8.2(15)	14.5(15)	25.5(15)	33.4(15)	53.7(15)	90.7(15)
	2080s (%Increase)	5.4(26)	6.6(27)	8.9(25)	15.9(26)	27.9(26)	36.6(26)	58.8(26)	99.3(26)
	Current	5	6.1	8.3	14.7	25.8	33.9	54.5	92
20-yr	2050s (%Increase)	6(20)	7.2(18)	9.8(18)	17.4(18)	30.5(18)	40(18)	64.3(18)	108.7(18)
	2080s (%Increase)	6.4(28)	7.8(28)	10.6(28)	18.8(28)	33(28)	43.3(28)	69.5(28)	117.4(28)
	Current	6	7.3	9.8	17.5	30.7	40.2	64.7	109.2
50-yr	2050s (%Increase)	7.2(20)	8.8(21)	11.9(21)	21.1(21)	37(21)	48.6(21)	78.1(21)	132(21)
	2080s (%Increase)	7.7(28)	9.4(29)	12.7(30)	22.6(29)	39.6(29)	51.9(29)	83.4(29)	140.9(29)
	Current	6.7	8.1	11	19.6	34.3	45	72.3	122.1
100-yr	2050s (%Increase)	8.2(22)	9.9(22)	13.4(22)	23.9(22)	41.9(22)	55(22)	88.5(22)	149.4(22)
	2080s (%Increase)	8.7(30)	10.5(30)	14.3(30)	25.4(30)	44.5(30)	58.4(30)	93.9(30)	158.5(30)

**Table A16 – Current and predicted rainfall intensity and percentage of increase (in parentheses) at station R602K300**

Return Period (years)	Climate Conditions	Rainfall Duration (hours)							
		24	18	12	6	3	2	1	0.5
	Current	2.4	2.9	3.9	6.9	12.1	15.8	25.5	43
2-yr	2050s (%Increase)	2.6(8)	3.2(10)	4.3(10)	7.6(10)	13.3(10)	17.5(11)	28.1(10)	47.4(10)
	2080s (%Increase)	2.8(17)	3.4(17)	4.6(18)	8.2(19)	14.3(18)	18.8(19)	30.2(18)	51.0(19)
	Current	3.3	4	5.3	9.5	16.7	21.9	35.2	59.4
5-yr	2050s (%Increase)	3.7(12)	4.4(10)	6(13)	10.7(13)	18.7(12)	24.6(12)	39.5(12)	66.8(12)
	2080s (%Increase)	4.0(21)	4.8(20)	6.5(23)	11.5(21)	20.2(21)	26.6(21)	42.7(21)	72.1(21)
	Current	3.9	4.7	6.3	11.3	19.7	25.9	41.6	70.3
10-yr	2050s (%Increase)	4.4(13)	5.3(13)	7.2(14)	12.7(12)	22.3(13)	29.3(13)	47.1(13)	79.6(13)
	2080s (%Increase)	4.7(21)	5.7(21)	7.7(22)	13.8(22)	24.2(23)	31.7(22)	51.0(23)	86.1(22)
	Current	4.4	5.4	7.3	12.9	22.7	29.7	47.8	80.7
20-yr	2050s (%Increase)	5(14)	6.1(13)	8.3(14)	14.7(14)	25.8(14)	33.9(14)	54.4(14)	91.9(14)
	2080s (%Increase)	5.5(25)	6.6(22)	8.9(22)	15.9(23)	27.9(23)	36.7(24)	58.9(23)	99.5(23)
	Current	5.2	6.3	8.5	15.1	26.4	34.7	55.8	94.2
50-yr	2050s (%Increase)	5.9(13)	7.2(14)	9.7(14)	17.3(15)	30.3(15)	39.7(14)	63.8(14)	107.8(14)
	2080s (%Increase)	6.4(23)	7.8(24)	10.5(24)	18.7(24)	32.8(24)	43.1(24)	69.2(24)	116.9(24)
	Current	5.7	6.9	9.4	16.7	29.3	38.4	61.8	104.3
100-yr	2050s (%Increase)	6.6(16)	8(16)	10.8(15)	19.2(15)	33.6(15)	44.1(15)	70.9(15)	119.7(15)
	2080s (%Increase)	7.1(25)	8.6(25)	11.7(24)	20.8(25)	36.5(25)	47.9(25)	76.9(24)	129.9(25)

**Table A17– Calculation Procedure for the 2080s Time Period Using G6140954**

A (KM2)	0.20	0.20	0.20	0.20	0.20	0.20
C	0.46	0.46	0.46	0.46	0.46	0.46
I(mm/hr)	88.06	125.10	149.63	173.16	203.62	226.44
Q(m3/s)	2.25	3.20	3.83	4.43	5.21	5.79
D (m)	0.28	0.32	0.34	0.36	0.38	0.40
D (observed)	0.26	0.28	0.30	0.31	0.33	0.34
Change (%)	7.5	12.3	14.4	15.9	17.5	18.4

Here Q = peak flow (m<sup>3</sup>/s)

C = runoff coefficient

I = average precipitation intensity over a given duration for return period T (mm/hr)

A = basin area (km<sup>2</sup>)

D = diameter (m)

**Table A18 – Calculation Procedure for the 2080s Time Period Using K6034075**

A (KM2)	0.39	0.39	0.39	0.39	0.39	0.39
C	0.28	0.28	0.28	0.28	0.28	0.28
I(mm/hr)	113.46	177.86	220.50	261.40	314.34	354.01
Q(m3/s)	3.44	5.40	6.69	7.94	9.54	10.75
D (m)	0.31	0.37	0.40	0.43	0.46	0.48
D (observed)	0.28	0.33	0.36	0.38	0.40	0.42
Change (%)	9.4	11.7	12.5	13.0	13.5	13.8

Here Q = peak flow (m<sup>3</sup>/s)

C = runoff coefficient

I = average precipitation intensity over a given duration for return period T (mm/hr)

A = basin area (km<sup>2</sup>)

D = diameter (m)